The Astrophysical Journal, 584:339–356, 2003 February 10

SOME DIFFUSE INTERSTELLAR BANDS RELATED TO INTERSTELLAR C_2 MOLECULES[1]

J. A. Thorburn,[2] L. M. Hobbs,[2] B. J. McCall,[3] T. Oka,[2] D. E. Welty,[2] S. D. Friedman,[4] T. P. Snow,[5] P. Sonnentrucker,[4] and D. G. York[2]

Received 2002 August 8; accepted 2002 October 18

ABSTRACT

We have investigated the correlations between the equivalent widths of 21 selected diffuse interstellar bands (DIBs) and the corresponding interstellar column densities $N(C_2)$, $N(CN)$, and $N(CH)$, toward 53 stars with color excesses $0.11 \leq E(B-V) \leq 1.99$. The observational data were derived primarily from echelle spectra acquired at $R = 38,000$ as part of our extensive, continuing survey of the bands. All but six of the 53 final spectra show signal-to-noise ratios $\geq$800 at 5780 Å. The principal result presented here is that seven of the 21 bands prove to be examples of "the C_2 DIBs," a class of weak, narrow bands whose normalized equivalent widths $W_\lambda(X)/W_\lambda$ (λ6196) are well correlated specifically with $N(C_2)/E(B-V)$ via power laws. In contrast, the similarly normalized equivalent widths of the 14 other, well-known DIBs analyzed here are uncorrelated, or weakly anticorrelated, with $N(C_2)/E(B-V)$, to within the observational uncertainties. Thus, the polyatomic molecule(s) presumed to cause these seven C_2 DIBs may bear a direct chemical relation to C_2 that is not shared by the polyatomic molecules putatively responsible for the other 14 bands. The C_2 DIBs also show positive correlations with $N(CN)/E(B-V)$ and $N(CH)/E(B-V)$ in our particular sample of light paths, although generally with shallower slopes in the case of $N(CN)$ and with greater scatter in the case of $N(CH)$. Eleven additional C_2 DIBs are also identified but are not analyzed here. Among the 18 C_2 DIBs identified, four apparently have not been previously detected. The λ4963 band is generally the strongest of the 18 C_2 DIBs, while the λ4734 band shows the most sensitive correlation with $N(C_2)$.

Subject headings: ISM: lines and bands — ISM: molecules

1. INTRODUCTION

The strengths (i.e., the equivalent widths) of most diffuse interstellar bands (DIBs) are widely assumed to be approximately proportional to the column densities of one or more polyatomic interstellar molecules that have not yet been identified (Herbig 1995; Tuairisg et al. 2000; Walker et al. 2001). If lines of sight toward more reddened stars reflected only the presence of larger numbers of precisely identical, uniform clouds, then all column densities derived from interstellar absorption lines, whether atomic, diatomic, or polyatomic in origin, would correlate with each other and with interstellar reddening linearly, and without any scatter at all. In our current ignorance of which molecules give rise to the observed DIBs, the subset of poorly correlated DIBs found in nature may present especially useful opportunities to investigate empirically how the strengths of various DIBs depend upon the differing total volume densities, radiation fields, and other physical conditions that are encountered in a large array of interstellar clouds. That is, the variable ratios of some DIB strengths from cloud to cloud must reflect the differing cloud environments but in a way not yet understood. Not only the total fractional abundances but also the ionization and the excitation equilibria of the postulated polyatomic molecules may be important in controlling the DIB strengths (Sonnentrucker et al. 1997; Vuong & Foing 2000).

The observed strengths of some DIBs correlate rather well with each other. Among many examples, two are the relatively weak, narrow pair λ5512/λ4984 (Fig. 1*a*) and the much stronger, broader pair λ5705/λ5780 (Fig. 1*b*), where the truncated wavelengths identify the respective bands. In contrast, other DIB pairs correlate poorly or not at all; one example among the bands just noted consists of the weak λ5512 band and the strong λ5780 band. The lack of correlation between these two particular DIBs is shown in Figure 1*c*, where a substantial dispersion of the λ5512/λ5780 ratio is evident toward various subsets of stars in our present survey that show, respectively, nearly identical values of the interstellar reddening. (A similar result is obtained when the strength of either individual line, for example, is chosen as the independent variable, in place of the reddening.) This result follows despite the fact that the strength of each of these two bands increases nearly linearly with increasing $E(B-V)$ but with extensive scatter about each of the mean relations. Because more values of $E(B-V)$ than of $N(H) = N(H\,I) + 2N(H_2)$ have been measured for the stars in our observing program, we will use the reddening as a substitute for the total column density of hydrogen (Bohlin, Savage, & Drake 1978), although the latter may be more precisely related to the DIB strengths.

Like the DIB strengths, the column densities of the diatomic interstellar molecules C_2, CN, and CH can vary widely among various light paths with nearly identical values of $N(H)$ and $E(B-V)$. In addition, these diatomic column densities are generally observed to vary nonlinearly with reddening and with each other (Federman et al. 1994). The average fractional abundances of these diatomic molecules along an interstellar light path are measured by $N(C_2)/N(H)$ or (approximately) $N(C_2)/E(B-V)$, for

[1] Based on observations obtained with the Apache Point Observatory 3.5 m telescope, which is owned and operated by the Astrophysical Research Consortium.

[2] Department of Astronomy and Astrophysics, University of Chicago, 5640 South Ellis Avenue, Chicago, IL 60037.

[3] Department of Astronomy, University of California at Berkeley, 601 Campbell Hall, Berkeley, CA 94720-3411.

[4] Department of Physics and Astronomy, Johns Hopkins University, 34th and Charles Streets, Baltimore, MD 21218.

[5] University of Colorado, CASA-Campus Box 389, Boulder, CO 80309.

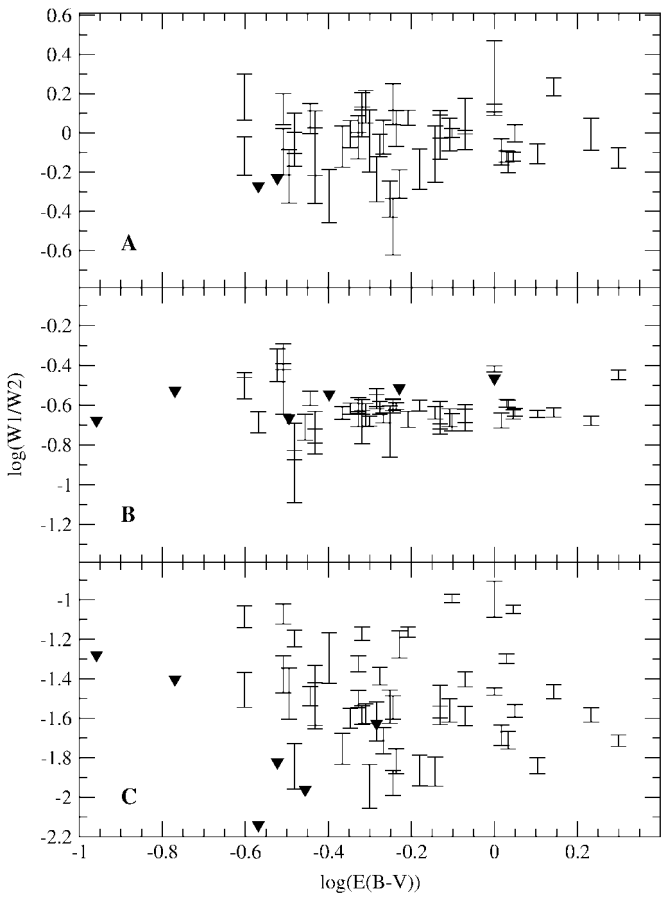

FIG. 1.—(*a*) Log[$W_\lambda(5512)/W_\lambda(4984)$] vs. log[$E(B-V)$]; (*b*) log[$W_\lambda(5705)/W_\lambda(5780)$] vs. log[$E(B-V)$]; (*c*) log[$W_\lambda(5512)/W_\lambda(5780)$] vs. log[$E(B-V)$]. All panels have a vertical range of 1.4 dex, and the triangles indicate upper limits. The scatter of data in (*a*) and (*b*) is largely explained by the observational error alone, while the scatter in (*c*) is substantially more than could be produced by the expected errors.

example. Such abundances can serve as observable indicators of the "average" physical conditions found among the various clouds present along a light path. In contrast to the unidentified DIB absorbers, the complex abundance variations observed for the simpler C_2, CN, and CH molecules have been extensively studied theoretically as well as observationally, and they are partially understood in terms of the physical conditions and the resulting chemical reaction networks in diffuse interstellar clouds (van Dishoeck & Black 1986).

It may be instructive to investigate how the strengths of various DIBs correlate with the average diatomic abundances (Krełowski et al. 1999) and thereby to study indirectly how the DIB strengths depend upon the various cloud environments. The purpose of the present paper is to present some new observational data concerning such connections, including those involving several previously unreported DIBs that prove to have distinctive properties.

2. THE OBSERVATIONS

2.1. *Instrumental Setup and Data Reduction*

The spectra for this program were obtained at various times from 1999 to 2002 with the 3.5 m telescope and ARC echelle spectrograph (ARCES) at Apache Point Observatory. Some other related results derived from this survey have been reported previously by McCall et al. (2001, 2002), Snow et al. (2002), and Oka et al. (2003). The ARCES spectrograph employs an echelle grating, two cross-dispersing prisms, and a SITe CCD detector with a 2048 × 2048 grid of 24 μm pixels (Wang et al. 2003). The width and length of the entrance slit on the sky are 1.″6 and 3.″2, respectively. Each exposure provides nearly complete spectral coverage from about 3500 to 10,000 Å, at a resolving power $R = \lambda/\Delta\lambda = 38{,}000$ or a velocity resolution of about 8 km s^{-1}. The resolution $\Delta\lambda$ refers to the FWHM of the instrumental profile, which spans 2.2 pixels on the detector. The absolute sensitivity of the instrument (including the effects of atmospheric transmittance) varies substantially over this wide wavelength range, reaching a broad maximum centered at approximately 6600 Å for a typical, reddened, early-B star in our program.

The maximum signal-to-noise ratio (S/N) that can be achieved near 5780 Å in a single exposure is approximately 500, a limit set by the nonlinearity of the detector at sufficiently high exposures. In an attempt to achieve the desired S/N > 1000 at 5780 Å in the final, summed spectrum of each program star, at least four individual exposures of each star were therefore obtained and subsequently combined during data reduction. At $V = 7.0$, the total exposure time required for four exposures was about 70 minutes under good observing conditions. The reduction of the spectra was carried out using the echelle package in NOAO's Image Reduction and Analysis Facility (IRAF), with several modifications to standard procedures.

Two difficulties can arise when an ARCES exposure is reduced in IRAF, both of which may be avoided by careful attention to parameter tuning. Owing to the scale of 0.″53 pixel^{-1} at the CCD, each order of a typical stellar exposure effectively extends over only 3 or 4 pixels along CCD columns, transverse to the echelle grating dispersion. In addition, the individual echelle orders are appreciably curved in their path along the direction of the CCD rows. Their cumulative displacement amounts to about 30 rows over the utilized width of the CCD. Due to both the narrowness of the echelle orders and their marked curvature, standard-order extraction techniques in IRAF, which do not include full fractional pixel weighting, will often produce nonnegligible sampling noise in the resulting one-dimensional spectra. Similar effects are well documented in other instruments (e.g., Space Telescope Imaging Spectograph, as discussed in Leitherer et al. 2001) and are commonly overcome by dithering the source light along the length of the entrance aperture. Although dithering is not possible for ARCES, the sampling noise can be minimized by suitably interpolating the fluxes between pixels along the CCD columns, before extraction of an order to its one-dimensional form. This technique in effect forces fractional pixel weighting for entire order profiles, rather than simply in the regions of low signal.

In the direction transverse to the dispersion, the wavelength-dependent separation between the centers of adjacent spectral orders reaches a minimum near 8000 Å. This minimum gap corresponds to 5.″0 on the sky, and an entrance slit with a length that corresponds to 3.″2 is consequently used to prevent overlapping of the orders. Except during the best seeing, the transverse extensions of an order in the stellar and the flat-field lamp exposures are therefore not greatly different, and the profile of a lamp exposure

along a CCD column also departs significantly from an ideal, nearly rectangular shape. Both characteristics of ARCES adversely affect standard, two-dimensional flat-fielding. These problem can be minimized by employing one-dimensional flat-fielding, in which both the stellar and the lamp exposures are extracted to one-dimensional form before their subsequent mutual division. This unconventional approach is also preferred on the basis of the sampling noise discussed above, because quotients of two mildly undersampled images are more adversely affected by sampling noise than is either individual image. Although one-dimensional flat-fielding is not expected to be as effective in eliminating fixed pattern noise, we have achieved maximum S/N of up to 2000 at 5780 Å in fully reduced, multiple, summed stellar spectra.

Continuum fitting of the data comprising the extracted, flat-fielded orders was accomplished by using eighth-order Legendre polynomials. A nonstandard method was used only in the case of the λ5780 band, where the extended absorption that flanks the DIB on both sides spanned appreciable parts, or all, of each of three orders. These three continuum profiles were estimated instead by interpolation across this gap between the many other orders.

2.2. *The Program Stars and the Spectra*

Some stellar data are listed in Table 1 for the 53 stars selected from our wider observing program for the investigations reported in this paper. The stellar photometry and the MK spectral types are generally those given in the Bright Star Catalogue or its Supplement or, for the fainter stars, in the *Hipparcos* Input Catalogue. The data for HD 37903, HD 46202, HD 46711, HD 50064, HD 166734, HD 168076, HD 172028, HD 229059, Cyg OB2 5, and HD 210121 were taken from other sources in the literature. The calculated color excesses $E(B-V)$ are based on the intrinsic colors of Johnson (1963). The distances to 11 of the stars are derived from *Hipparcos* parallaxes with 4 σ precision or better. The spectroscopic distances determined for the remaining 42 stars are based on either (1) the calibration by Blaauw (1963) of MK spectral types in terms of absolute visual magnitude, along with an assumed value $R_V = A_V/E(B-V) = 3.1$ or (2) membership in a cluster or OB association. The fractional accuracy of these distances is uncertain and probably varies widely among the program stars, but may typically be about 25% (or 4 σ). All but six of the 53 final, summed spectra produced S/N $\geq$800 at 5780 Å, as shown in the last column of the table. A large number of generally bright, narrow-lined stars with well-determined MK spectral types of classes O, B, and early A were also observed, in order to identify the stellar lines expected in the spectra of our program stars. Some bright, broad-lined stars were observed in order to identify the many telluric lines that contaminate the spectra.

Two requirements were used to select these program stars. First, for all but three relatively highly reddened stars, reliable interstellar column densities of both CN and CH were generally taken from the literature or, usually at a higher S/N but lower resolution, from our spectra when necessary. A small number of these results take the form of upper limits only. In addition, column densities of C_2 were derived in all cases from our spectra, in order to provide a data set that is as homogeneous as possible. Toward 19 of the 53 stars, only upper limits on C_2 were obtained. Definite column densities of all three diatomic molecules together are found here in 31 of the 53 directions.

Second, the equivalent widths of 32 selected DIBs of widely ranging types, which are listed in Table 2, were also derived from our spectra. These DIBs will be discussed below, and 21 of them (those not noted) in Table 2 will be analyzed in more detail. Toward a number of the less reddened stars, only upper limits are available for some of the intrinsically weaker DIBs included in Table 2. However, the DIBs found at 4963 and 4984 Å, which will prove to be especially valuable in the analysis below, were positively detected in the spectra of all but four of the 53 stars. The wavelengths and the bandwidths listed in Table 2 are taken from the literature or, in the cases of the four newly discovered DIBs, from our spectra of HD 204827. For these four DIBs, the wavelengths were measured relative to the interstellar K I λ7699 line, and no corrections (which amount to -0.02 Å or less) for instrumental broadening were made to the measured bandwidths.

The measured equivalent widths of the DIBs, as well as the derived or adopted column densities of C_2, CN, and CH, are collected in the Appendix. Where differences exist, the DIB strengths given here for HD 183143 supersede those reported previously by Snow et al. (2002). To illustrate both the general features of the DIBs and the quality of our spectra, Figure 2 shows the 32 DIBs of Table 2 in the spectra of HD 183143 and HD 204827, two stars with similar, large color excesses, $E(B-V) = 1.27$ and 1.10, respectively. The DIBs found in the spectrum of HD 183143 have been studied extensively (Herbig 1995), while the light path to HD 204827 shows the largest value of $N(C_2)$ among our 53 program stars, as well as the largest value of $N(C_3)$ among the 24 stars examined by Oka et al. (2003). The measured equivalent widths of the diffuse bands in these two spectra are given in Table 3; the filled circles flanking the λ5780 DIB in Figure 2 indicate the wavelength limits within which the equivalent widths of this DIB were calculated (Krełowski & Sneden 1993). The synthetic DIB spectrum of Tuairisg et al. (2000) is also plotted in the upper panel of Figure 2, for comparison.

To assist in identifying the many stellar lines present in the spectra of HD 204827 (B0 V, Table 1) and HD 183143 (B7 Iae, Table 1), our spectra of 10 Lac (O9 V) and β Ori (B8 Iae) are also presented in the bottom panel. Note that the stellar lines of 10 Lac, such as C IV λ5801, are considerably narrower than their counterparts in the spectrum of HD 204827. (A relatively small contribution to this difference arises from the facts that HD 204827 is a short-period, double-lined binary whose stellar lines shift with respect to the DIBs, and that four different nights of data for the star were combined to produce Fig. 2.) The intrinsically stronger DIBs, such as λ5780, are clearly present as well in the spectrum of 10 Lac, which shows $E(B-V) = 0.11$. Telluric lines have not been removed from the plots of our spectra in Figure 2, as is evident in the region of the λ6284 DIB, for example. These lines appear double in the spectrum of β Ori because spectra of the star obtained on two different nights were combined.

Many of the DIBs present in Figure 2, including λ4762, λ6113, and λ6445 for example, show narrower profiles toward HD 204827 than toward HD 183143. Although the atomic interstellar lines of K I seen toward both stars at high resolution reveal several distinct intervening clouds, the

TABLE 1
THE STARS OBSERVED

HD	Name	V	$B-V$	MK	$E(B-V)$	d (pc)	S/N
20041		5.79	0.73	A0 Ia	0.72	1400	605
21483		7.06	0.36	B3 III	0.56	440	1000
21389		4.54	0.56	A0 Iae	0.57	940	1000
23180	o Per	3.83	0.05	B1 III	0.31	280	1037
281159		8.51	0.69	B5 V	0.85	240	627
24398	ζ Per	2.85	0.12	B1 Ib	0.31	301	1000
24534	X Per	6.10	0.29	O9.5pe	0.59	590	980
24912	ξ Per	4.04	0.01	O7e	0.33	470	1240
26571		6.12	0.19	B9 IIIp	0.25	140	1400
27778	62 Tau	6.36	0.17	B3 V	0.37	223	1171
29647		8.31	0.91	B8 IIIp	1.00	177	1000
30614	α Cam	4.29	0.03	O9.5 Iae	0.30	820	1324
34078	AE Aur	5.96	0.22	O9.5 Ve	0.52	620	976
35149	23 Ori	5.00	−0.15	B1 V	0.11	450	1028
36371	χ Aur	4.76	0.34	B5I ab	0.43	880	1435
37061		6.83	0.26	B1 V	0.52	580	976
37903		7.83	0.10	B1.5 V	0.35	910	910
41117	χ2 Ori	4.63	0.28	B2 Iae	0.45	1000	1323
42087	3 Gem	5.75	0.21	B2.5 Ibe	0.36	1200	1044
43384	9 Gem	6.25	0.45	B3 Ib	0.58	1100	1001
46202		8.19	0.18	O9 V	0.49	2000	825
46711		9.10	0.86	B3 II	1.04	1200	1100
48099		6.37	−0.05	O6e	0.27	1600	803
50064		8.25	0.78	B6 Ia	0.85	3400	1000
53367		6.96	0.44	B0 IVe	0.74	780	990
147888	ρ Oph D	6.74	0.31	B5 V	0.47	136	1039
147889		7.90	0.83	B2 V	1.07	136	904
147933	ρ Oph A	5.02	0.24	B2 IV	0.48	121	954
149757	ζ Oph	2.56	0.02	O9.5 V	0.32	140	1565
166734		8.41	1.08	O8e	1.39	720	750
167971		7.45	0.77	O8e	1.08	730	1083
168076		8.21	0.46	O5f	0.78	2100	624
169454		6.61	0.94	B1.5 Ia	1.12	930	1807
170740		5.72	0.24	B2 V	0.48	213	1199
172028		7.83	0.55	B2 V	0.79	380	800
179406	20 Aql	5.34	0.13	B3 V	0.33	160	1485
183143		6.86	1.22	B7 Iae	1.27	1000	1081
185418		7.45	0.22	B0.5 V	0.50	950	1100
186994		7.50	−0.13	B0 III	0.17	2500	1000
192639		7.12	0.35	O8e	0.66	1100	966
229059		8.70	1.53	B1.5 Iap	1.71	1000	883
	Cyg OB2 5	9.10	1.67	O7f	1.99	1700	316
198478	55 Cyg	4.84	0.41	B3 Iae	0.54	980	1039
199579		5.96	0.05	O6 Ve	0.37	1200	1199
203938		7.08	0.46	B0.5 IV	0.74	700	1020
204827		7.94	0.81	B0 V	1.11	600	2000
206165	9 Cep	4.73	0.30	B2 Ib	0.47	620	1000
206267		5.62	0.21	O6f	0.53	1000	2600
207198		5.95	0.31	O9 IIe	0.62	1000	1700
210121		7.67	0.20	B3 V	0.40	210	1000
210839	λ Cep	5.04	0.25	O6 If	0.57	505	1008
218376	1 Cas	4.85	−0.03	B0.5 IV	0.25	339	1050
	BD+63 1964	8.46	0.71	B0 II	1.00	1400	514

radial-velocity range of the stronger of these clouds seen toward HD 183143 (about 24 km s^{-1}) exceeds that toward HD 204827 (about 12 km s^{-1}) by only 1.5 resolution elements in our spectra. Therefore, the difference in cloud multiplicity does not appear to be the primary cause of the observed difference in the widths of some DIBs; the effect appears to be largely intrinsic to the DIBs and to the respective environments in which they are formed. Furthermore, such a difference is largely absent in some of the other DIBs, such as λ6203.

The quality of our data can be further illustrated by a comparison of two relatively strong DIBs, for each of which the random fractional errors of measurement are relatively small. Figure 3 shows the correlation between the equivalent widths of the λ5780 and λ5705 DIBs in the spectra of the 53 program stars (cf. Fig. 1*b*). The linearity in this relation as

TABLE 2
SOME PROPERTIES OF 32 DIBs

λ (Å)	σ (Å)	FWHM (Å)	Reference	C_2 DIB?
4363.77[a]	0.02	0.46	New	Yes
4726.27[a]	0.04	0.99	3	Yes; blend
4734.73	0.02	0.40	New	Yes
4762.57	0.10	2.10	3	No
4963.96	0.02	0.62	5	Yes
4969.12[a]	0.03	0.80	1	Yes
4979.58[a]	0.03	0.61	New	Yes
4984.73	0.04	0.53	5	Yes
5003.62[a]	0.03	0.66	New	Yes
5170.44[a]	0.02	0.43	7	Yes
5175.99	0.03	0.71	7	Yes
5418.91[a]	0.05	0.80	7	Yes; blend
5512.62	0.03	0.48	1, 7	Yes
5541.77[a]	0.04	0.60	5	Yes
5544.97	0.05	0.79	3	No
5546.46[a]	0.03	0.56	1, 7	Yes
5705.13	0.11	2.15	2	No
5762.74[a]	0.05	0.51	4	Yes
5769.08	0.04	0.58	4	Yes
5780.59	0.05	2.07	6	No
5793.14[a]	0.04	0.95	9	Yes
5797.11	0.05	0.97	6	No
6113.22	0.03	0.65	3	No
6196.00	0.03	0.65	2	No
6203.08	0.03	3.93	1, 3	No
6270.06	0.33	1.03	3	No
6284.31	0.33	2.58	6	No
6376.06	0.03	0.74	3	No
6379.27	0.08	0.79	3	No
6425.70	0.03	0.71	1, 3	No
6613.72	0.12	1.14	6	No
6729.28	0.03	0.46	1, 8	Yes

[a] Not included in the correlation studies. These DIBs are blended with stellar lines at some spectral types, or with other DIBs, or they are relatively weak.

REFERENCES.—(1) Galazutdinov et al. 2000; (2) Herbig 1967; (3) Herbig 1975; (4) Jenniskens & Désert 1993; (5) Jenniskens & Désert 1994; (6) Merrill 1934; (7) Tuairisg et al. 2000; (8) Weselak, Schmidt, & Krełowski 2000; (9) Krełowski, Sneden, & Hiltgen 1995.

TABLE 3
MEASUREMENTS FOR HD 183143 AND HD 204827

λ (Å)	183143	1 σ Error	204827	1 σ Error
C_2 DIBs: Equivalent Widths (mÅ)				
4363.77[a]	<3	...	13.5	1
4726.27[a]	Blend	...	Blend	...
4734.73	<2	...	15.4	1
4963.96	26	1	55	1
4969.12[a]	11.2	1.5	16.2	1
4979.58[a]	<2	...	13.4	1
4984.73	14	1	30.4	1
5003.62[a]	<4	...	18.5	1
5170.44[a]	<10	...	11.2	1
5175.99	<3	...	37.4	1
5418.91[a]	9.7	1	48	1
5512.62	11	1	23	1
5541.77[a]	12	1	16.5	1
5546.46[a]	3.5	0.7	19.4	1
5762.74[a]	5.6	1	12.1	1
5769.08	<3	...	19.3	1
5793.14[a]	5.5	1	18.1	1
6729.28	9	3	17	1.2
Other DIBs: Equivalent Widths (mÅ)				
4762.57	122	7	49	2
5544.97	32	2	29.4	1
5705.13	172	7	58	3
5780.59	758	8	257	4
5797.11	295	10	199	3
6113.22	39	2	23.6	1
6196.00	92	2	41.5	1
6203.06	350	11	116	4
6270.06	268	10	82	5
6284.31	1930	150	518	60
6376.06	58	2	45	2
6379.27	113	3	96	1.5
6425.72	26	1	16	1
6613.72	337	4	171	3
Column Densities (1e12 cm^{-2})				
$N(C_2)$	<6	...	440	29
N(CH)	50	3	80	10
N(CN)	2.2	0.3	55	5

[a] Not included in the correlation studies. These DIBs are blended with stellar lines at some spectral types, or with other DIBs, or they are relatively weak.

both bands vary in strength by a factor of at least 8 shows that the strong λ5780 DIB remains unsaturated up to equivalent widths near 800 mÅ.

3. DIBs AND C_2

Initial inspections of our spectra showed that, in contrast to many broader, stronger DIBs, the equivalent widths of some narrow, weak DIBs increase on average with the column density $N(C_2)$, at various approximately fixed (and relatively large) values of the color excess. That is, the strengths of some DIBs do correlate specifically with $N(C_2)$, in addition to $E(B-V)$. For this reason, we will refer to this class of diffuse bands as "the C_2 DIBs" (Table 2). The C_2 DIBs may bear a direct chemical relation to C_2 that is not shared by the other bands considered here. Alternatively, both the C_2 molecules and the molecules presumed to cause the C_2 DIBs may form and survive efficiently under very similar physical conditions, without a direct chemical relation. In addition, Oka et al. (2003) have recently reported detections of interstellar C_3 molecules toward 15 stars, and these data reveal a very close correlation between $N(C_2)$ and $N(C_3)$. Thus, the strengths of the C_2 DIBs correlate well with the column densities of each of the two simplest molecules that consist of pure carbon chains.

As an illustration of these effects, we further compare HD 183143 and HD 204827 (Fig. 2 and Table 3). The value of $N(C_2)$ toward HD 204827 exceeds that toward HD 183143 by a factor of at least 68. In concert, the strength of the λ4734 DIB is seen to increase by a factor of at least 7.7, while that of the λ6270 DIB decreases by a factor of 0.32. The ratio $W_\lambda(4734)/W_\lambda(6270)$ therefore increases by a factor of at least 25, which is crudely comparable to the corresponding $N(C_2)$ ratio and entirely different from the ratio, 0.87, of the two color excesses. We emphasize again that, in our representative sample of light paths that includes wide ranges of reddening and of C_2 column density, the strengths

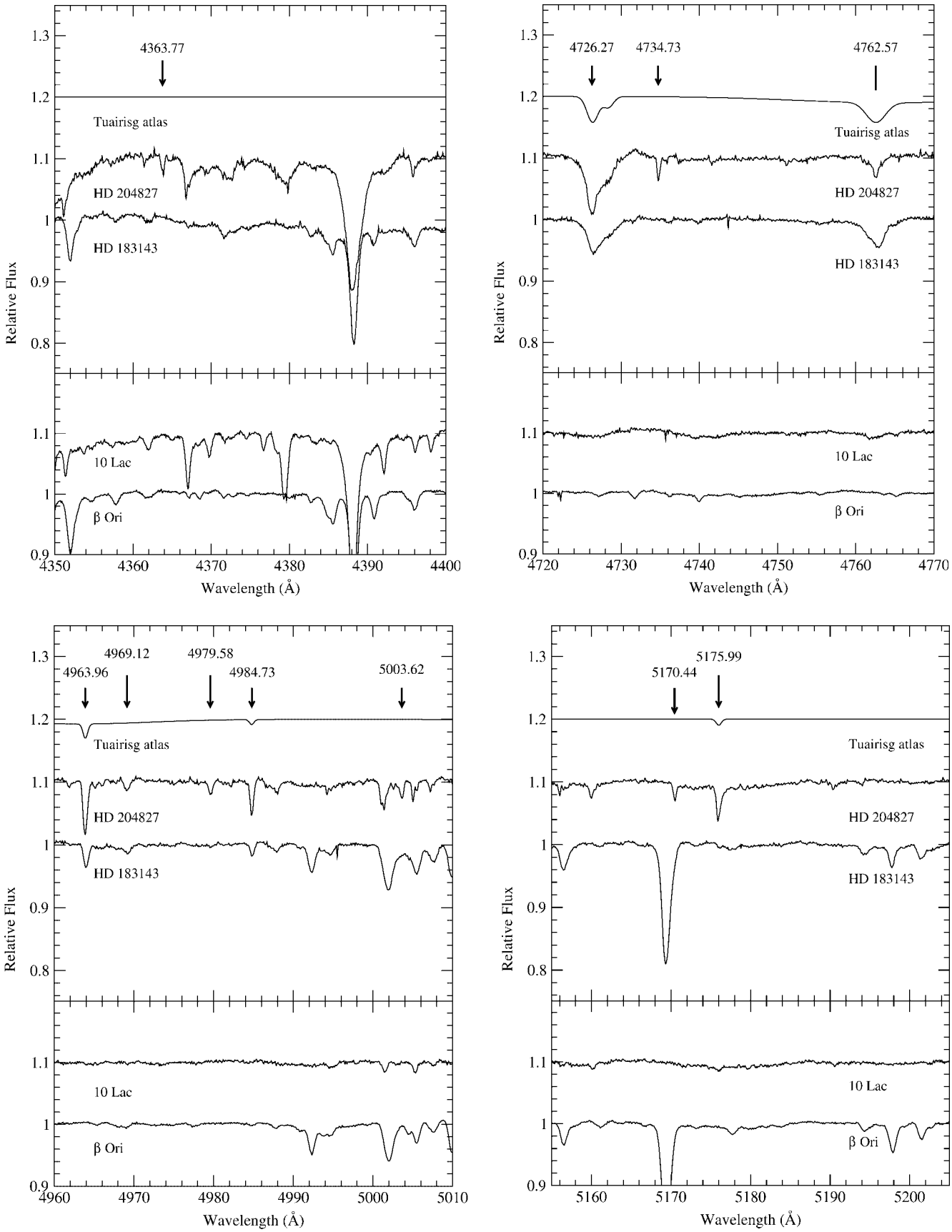

FIG. 2.—Spectra of HD 183143 and HD 204827, along with the synthetic spectrum of the Tuairisg et al. (2000) atlas, in the vicinity of 32 DIBs considered in this paper. The 18 C_2 DIBs are indicated by the arrows shown above the spectra, the other 14 DIBs by plain tick marks. The interstellar λ6707 line of Li I is also marked. Many stellar and telluric lines are also seen in the two stellar spectra. To facilitate the identification of the stellar lines, the spectra of two lightly reddened standard stars are presented in the lower panel (see the discussion in § 2.2). For clarity, vertical shifts of the spectra amounting to multiples of 0.1 unit of relative flux have been applied, as needed.

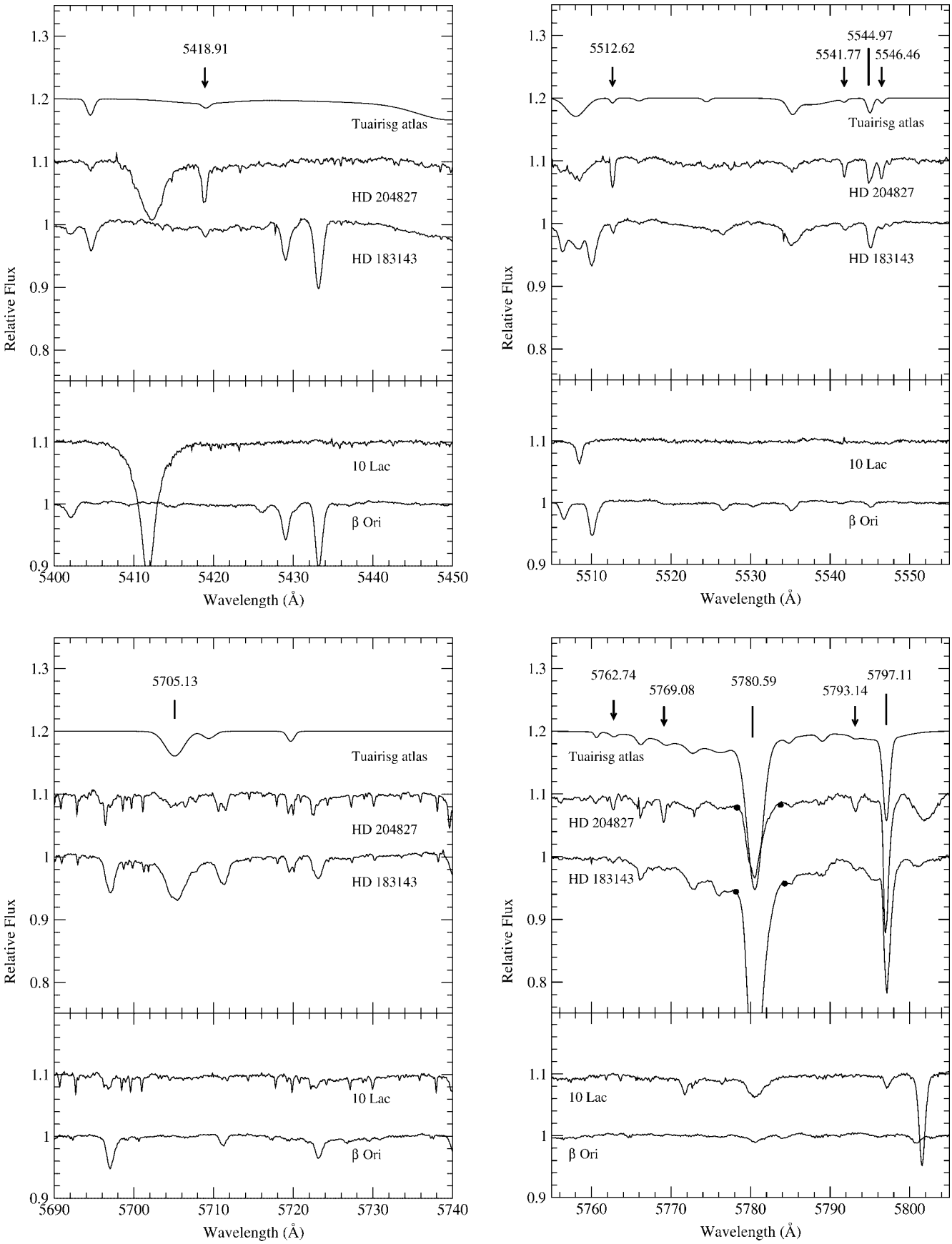

FIG. 2.—*Continued*

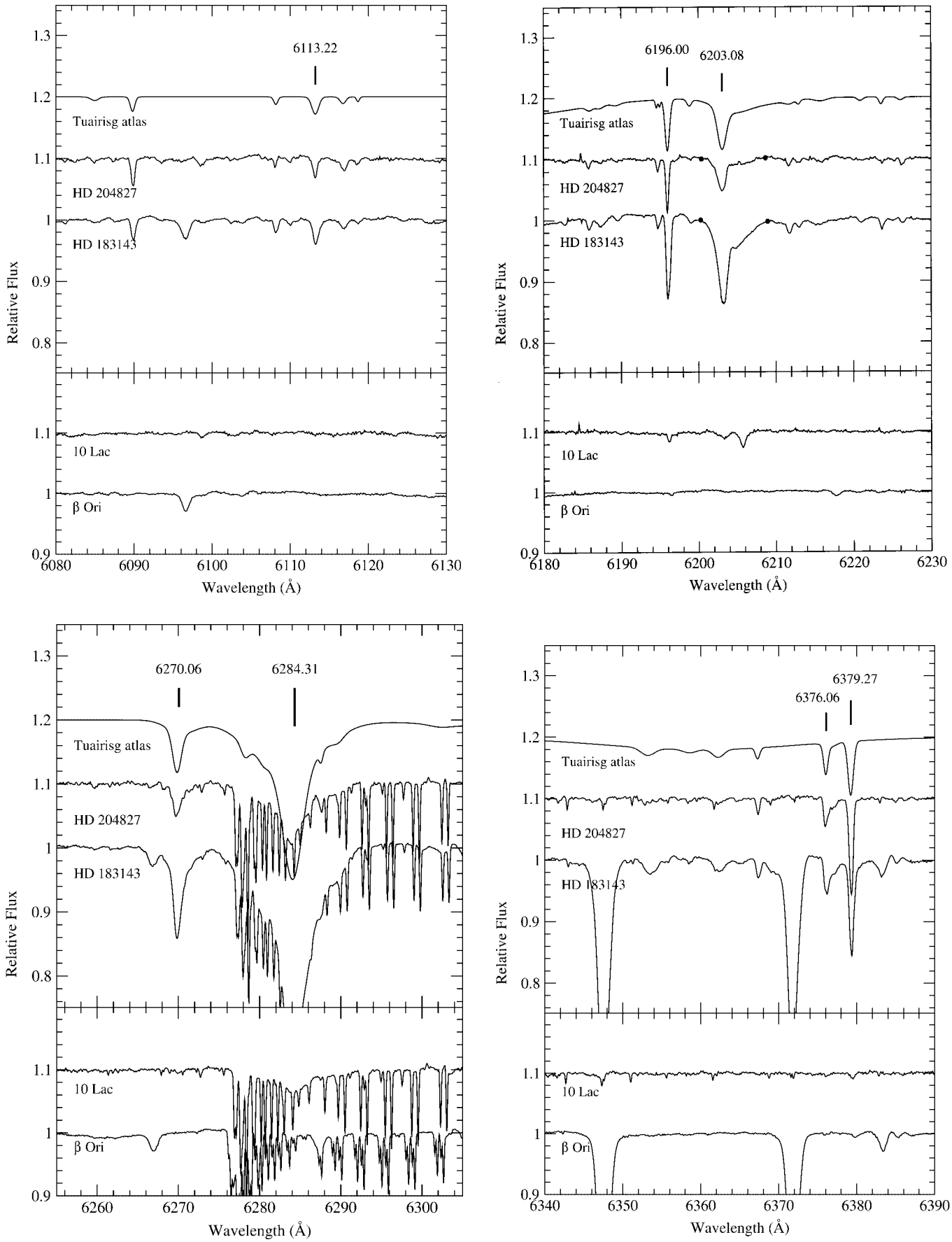

FIG. 2.—*Continued*

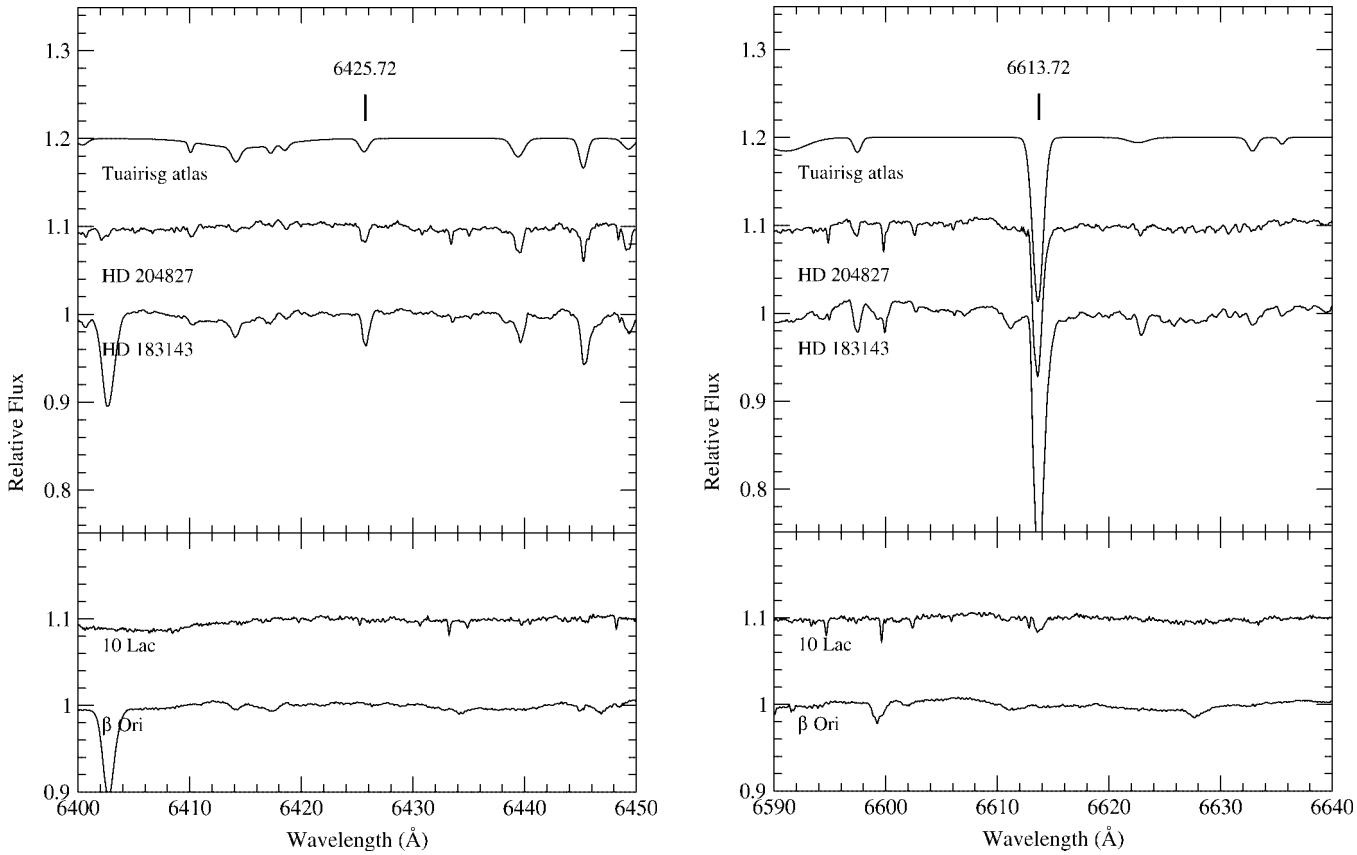

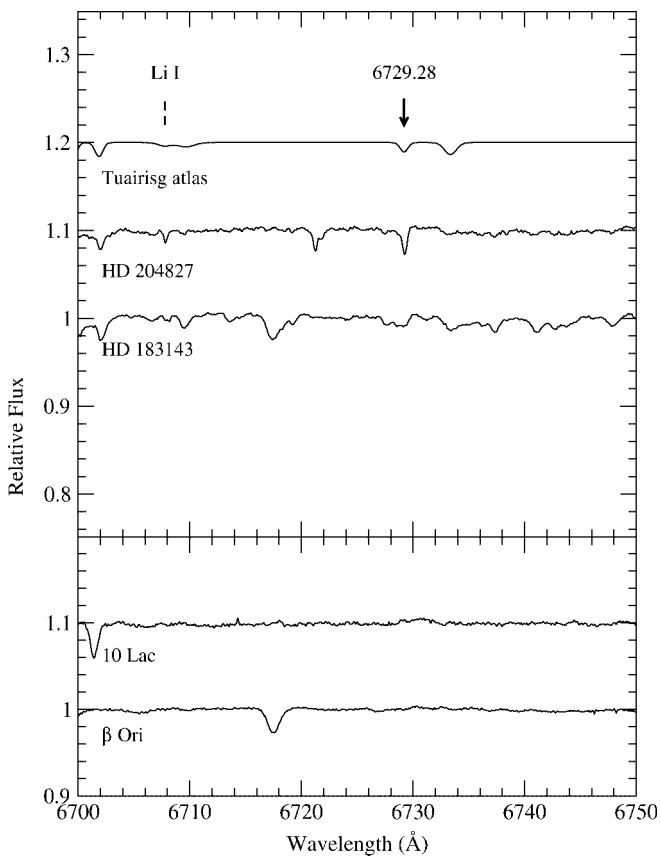

FIG. 2.—*Continued*

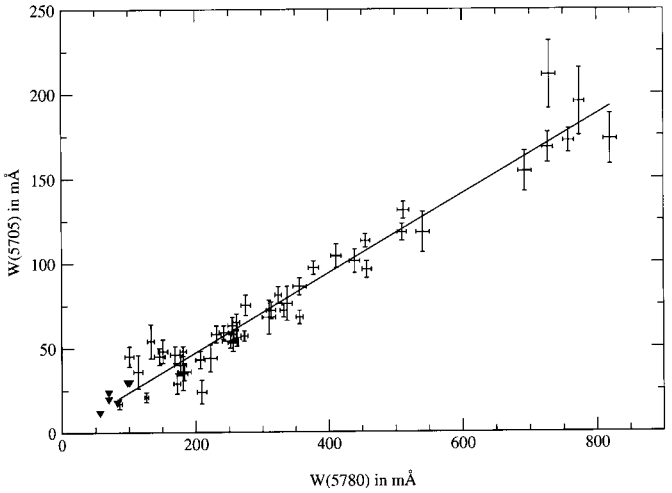

FIG. 3.—Plot of $W_\lambda(5705)$ vs. $W_\lambda(5780)$ for the 53 program stars. The solid line is a least-squares fit to the data for each of 47 stars toward which both bands were detected. The fitting line was not forced to pass through the origin.

of most other DIBS, such as λ6613 and λ6196 for example, show no mean trend with $N(C_2)$ at roughly fixed values of $E(B-V)$ but rather show scatter in such plots that exceeds the observational errors.

More precisely, it will often be preferable to compare not W_λ(DIB) and $N(C_2)$ but rather the ratio $W_\lambda(\mathrm{DIB})/W_\lambda(6196)$ as a function of $N(C_2)/E(B-V)$. At least approximately, this procedure cancels the nearly linear increases of the strengths of both DIBs with reddening. It also provides a normalized measure of a DIB's strength for comparison with the similarly normalized diatomic abundances, $N(C_2)/N(H)$ or $N(C_2)/E(B-V)$, which are of basic physical significance. In effect, such a choice of normalization provides a simplified form of a multivariate analysis. By definition, the C_2 DIBs are those for which the normalized band strengths increase on average with $N(C_2)/E(B-V)$. Conversely, for the strong, broad, well-known DIBs in Table 2, such as λ5780 and λ6284 for example, band strengths tend to be greatest when C_2 is undetectable and the color excess is high. The remaining DIBs of intermediate strength and width, such as λ6196, show no apparent sensitivity to $N(C_2)$, either alone or when normalized by color excess. For this reason, we have selected λ6196 as a relatively strong, easily measured DIB to use as a C_2-neutral, normalizing variable for the DIB equivalent widths in our correlation studies.

For each of 20 DIBs (of wavelength X, but excluding λ6196) not noted in Table 2, we therefore compared the values of $\log[W_\lambda(X)/W_\lambda(6196)]$ and $\log[N(C_2)/E(B-V)]$ for all program stars. Figure 4*a* shows the results for three illustrative bands, λ4734, λ6613, and λ6203. As we expected, the scatter about the fitting lines in the plots of these normalized variables is indeed smaller than that for the unnormalized variables $W_\lambda(X)$ versus $N(C_2)$ for almost all of the DIBs, and usually substantially so. Reweighted least-squares fits to these data plots were derived through use of the FORTRAN code PROGRESS (Rousseeuw & Leroy 1987). This method uses the least median of squares to improve the resistance of the regression lines to sufficiently outlying data points, by assigning zero weight to such points in the final fit. The uncertainty in a fitted slope was estimated in the usual way, via the variance matrix of the reweighted data set. All lower and upper limits in the data were excluded from the fits. Although the data points for the λ6613 and λ6203 DIBs are very crowded in it, Figure 4*b* better emphasizes the differences among the three slopes by utilizing the same vertical scale in all three panes.

The upper part of Table 4 summarizes the fitting parameters derived for each of the 20 normalized DIBs, arranged in order of the slopes against $N(C_2)/E(B-V)$ (col. [2]). The significance or robustness of the slope is indicated in column (3), where the ratio of the slope to its uncertainty is given. As another indication of how well determined is the slope, an estimate of the dispersion (in units of dex) of the data points about the fit appears in column (4). Finally, the usual correlation coefficient r is listed in column (5). The scatter for one band, λ5544, appreciably exceeded that for all of the others, and this led to the rejection of too many outlying points in this plot by the PROGRESS routine. A simple least-squares fit was therefore substituted instead, for this band only.

The slopes of the regression lines are found to exceed 0.3 for all seven C_2 DIBs in this sample. (The identification of these particular bands was originally achieved by simple inspection of the spectra, as in Fig. 2, however. The 11 additional C_2 DIBs listed in Table 2 have been identified so far only by similar inspection as well.) Except possibly for λ4734 and λ5769, the normalized strengths of the C_2 DIBs are seen to vary more slowly than linearly with $N(C_2)/E(B-V)$; for example, a square-root dependence obtains approximately for λ4984, λ6729, and λ4963. For some DIBs of weak or intermediate strength that are not C_2 DIBs, such as λ4762, and λ6113, the slope of the regression line vanishes, showing less than 2 σ significance. For some of the strongest DIBs, such as λ5780, λ6284, and λ6203, the slopes and the correlation coefficients both indicate an anticorrelation of slightly greater significance than 2 σ. As seen in Figure 4*a*, data points that have only upper limits on $N(C_2)$ occur along the extrapolated portion of the regression line calculated to fit the positive detections only. This finding, as well as the appearance of the spectra themselves (Fig. 2), reinforces the conclusion that the strong DIBs are relatively strongest where $N(C_2)/E(B-V)$ is lowest (Snow et al. 2002). With future, more extensive data of higher precision, or with a different stellar sample, many of the DIBs may move up or down in the ranking of Table 4 by a few places.

An additional, related trend is that the broadest DIBs, which are also generally the strongest DIBs, therefore have the most negative slopes against $N(C_2)/E(B-V)$. For example, each of the first 13 bands listed in Table 4 is narrower than each of the last seven, if uncertainties in the line widths and the slopes are ignored.

Along with λ5769, the DIB in Table 4 that shows the most sensitive variation in concert with the average C_2 abundance is λ4734, a band which apparently has not been previously detected. Because it is narrower and weaker than most of the previously known DIBs, this newly discovered band becomes conspicuous only when recorded at relatively high resolution and high S/N, and when seen along light paths with relatively high average C_2 abundances. The width of this DIB, 0.40 Å (Table 2), exceeds our instrumental resolution by a factor of only 3 and is therefore only partially resolved in our spectra.

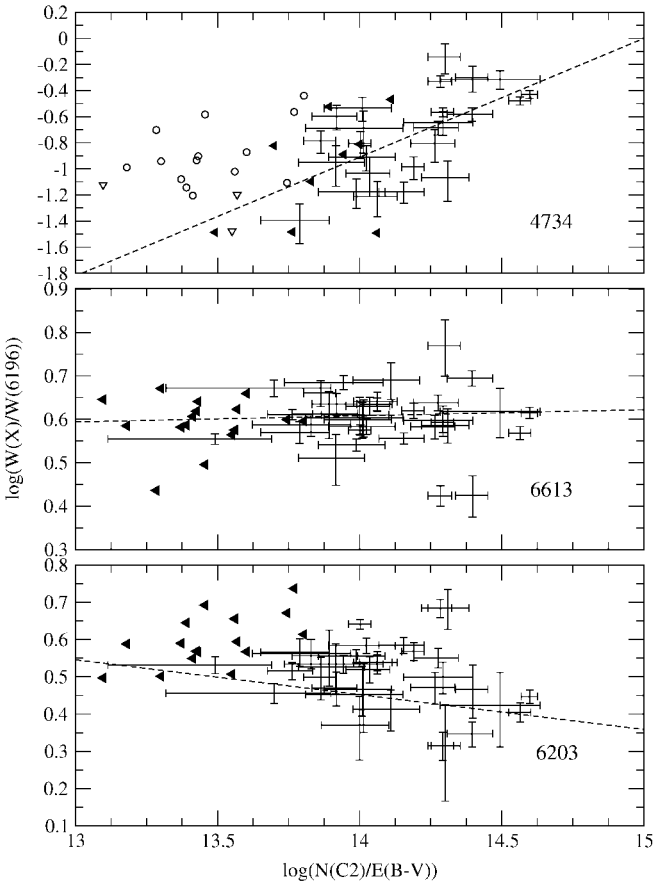

FIG. 4*a*

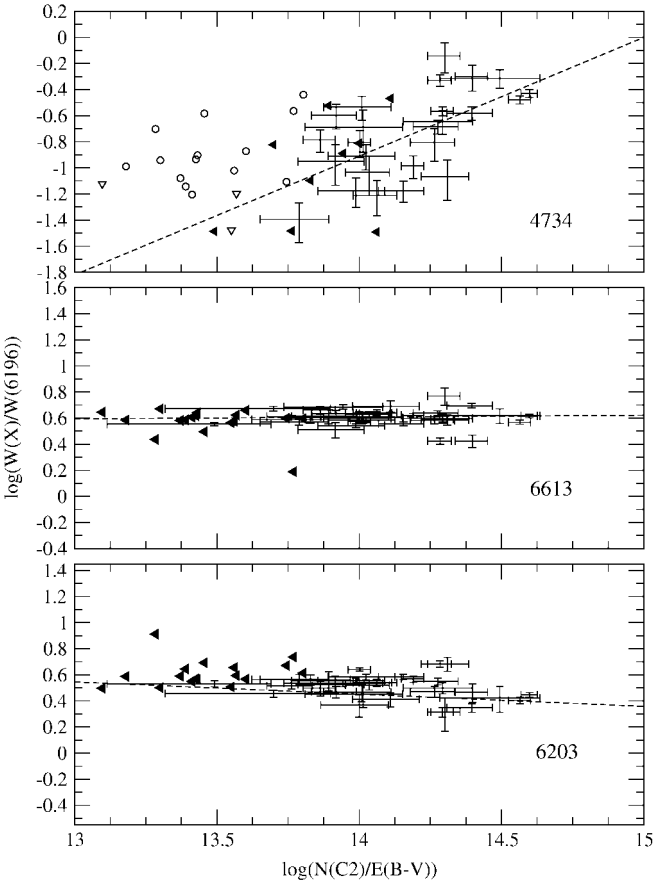

FIG. 4*b*

FIG. 4.—(*a*) Normalized DIB equivalent widths vs. $N(C_2)/E(B-V)$, with both variables plotted logarithmically. Note that the total range of the y-axis for the C_2 DIB λ4734 is 2 orders of magnitude, while it is appreciably less than 1 order of magnitude for the other two DIBS. Dashed lines depict the reweighted least-squares fits to the detections. The filled triangles indicate upper limits on $N(C_2)$, the open triangles, upper limits on $W_\lambda(4734)$, and the open circles, upper limits on both quantities. The errors are indicated by bars that extend over a full range amounting to 2 σ, or ± 1 σ. (*b*) Same as (*a*), except for the vertical scales, which cover 2 orders of magnitude in all panes.

The band's profile in the spectrum of HD 204827, where it reaches maximum strength in our sample, shows a relatively shallower long-wavelength wing but no other definite structural detail at our resolution.

Some properties of 11 other C_2 DIBs evident in our spectra that are not analyzed here are given in Table 2, where these DIBs are noted; three of these apparently have not been detected previously either. We will only briefly consider these other 11 C_2 DIBs in this paper. Each is blended with stellar lines, at least at some spectral types, or with other DIBs, or it is weaker than most of the seven C_2 DIBs listed in Table 2 and hence is affected by fractionally larger errors of measurement

4. OTHER RESULTS

4.1. *DIBs and* CN

Subsequent scrutiny of our spectra and of additional data taken from the literature revealed that generally similar results are found when CN is substituted for C_2 (see the Appendix). The values of the resulting "CN slopes" are listed in the middle section of Table 4 for comparison with those for C_2, and the illustrative plots in Figure 5 can be compared with those in Figure 4*a*. The ordering of the DIBs in Table 4 proves to be crudely similar with respect to C_2 and CN. For example, in the case of the λ6113 band and CN, the low significance of the slope, 1.049, and the low value of the correlation coefficient, $r = 0.175$, show that the corresponding slope has a large uncertainty. This band's nominally steep slope against CN is therefore likely to be spurious.

As is seen in Figure 6, the relation between $N(C_2)$ and N(CN) for our sample of interstellar light paths is linear, to within the large uncertainty in the slope. Extensive scatter is present about the mean trend, however, and the generally good agreement in detail between corresponding plots like those shown in Figures 4 and 5 therefore does not follow automatically. At least within the range of cloud environments included within our sample, this agreement consequently suggests a fairly close chemical connection among C_2, CN, and the polyatomic molecule(s) presumably responsible specifically for the C_2 DIBs. Alternatively, all three (or more) species may form and survive under very similar physical conditions.

4.2. *DIBs and* CH

Along with additional data from the literature, our spectra were also used to investigate correlations between the

TABLE 4

LEAST-SQUARES FITS[a]

DIB (1)	Slope (2)	Significance (3)	Scatter (4)	r (5)	Degrees of Freedom (6)	Rank (7)
			Versus $N(C_2)/E(B-V)$			
4734	0.910	3.750	0.263	0.616	23	1
5769	0.896	5.721	0.170	0.795	23	2
5175	0.761	4.021	0.276	0.579	32	3
4984	0.529	4.329	0.178	0.608	32	4
6729	0.520	3.459	0.209	0.547	28	5
4963	0.516	6.521	0.115	0.771	32	6
5512	0.307	2.550	0.163	0.428	32	7
6113	0.272	1.030	0.233	0.182	31	8
5544	0.192	2.844	0.097	0.455	31	9
6425	0.180	1.658	0.154	0.290	30	10
5797	0.120	2.076	0.084	0.349	32	11
6379	0.117	1.257	0.134	0.220	32	12
6376	0.106	1.811	0.082	0.314	32	13
4762	0.077	0.643	0.164	0.118	29	14
6613	0.014	0.429	0.044	0.079	32	15
6270	−0.002	0.028	0.109	0.000	29	16
5780	−0.072	2.198	0.047	−0.372	32	17
6284	−0.142	2.013	0.103	−0.335	32	18
6203	−0.144	2.804	0.073	−0.456	32	19
5705	−0.179	2.556	0.098	−0.435	28	20
			Versus $N(CN)/E(B-V)$			
4734	0.505	5.640	0.210	0.769	24	2
5769	0.261	2.230	0.251	0.446	21	7
5175	0.444	5.158	0.228	0.680	34	3
4984	0.304	4.796	0.185	0.630	35	5
6729	0.369	3.876	0.218	0.605	26	4
4963	0.277	6.101	0.127	0.739	36	6
5512	0.222	3.460	0.187	0.510	35	8
6113	0.648	1.049	0.484	0.175	35	1
5544	0.121	3.817	0.094	0.542	36	9
6425	0.040	0.932	0.122	0.162	35	13
5797	0.083	2.615	0.094	0.400	37	11
6379	0.074	1.391	0.155	0.229	37	12
6376	0.091	3.090	0.083	0.474	35	10
4762	−0.064	1.087	0.163	−0.183	34	16
6613	0.000	0.080	0.045	−0.028	37	14
6270	−0.088	2.396	0.102	−0.395	34	18
5780	−0.061	4.132	0.042	−0.584	37	15
6284	−0.145	5.714	0.072	−0.700	37	20
6203	−0.110	4.594	0.071	−0.613	37	19
5705	−0.074	2.399	0.084	−0.401	33	17
			Versus $N(CH)/E(B-V)$			
4734	1.284	4.021	0.319	0.612	27	3
5769	1.153	3.500	0.330	0.581	25	4
5175	1.406	4.258	0.330	0.568	40	1
4984	0.437	3.023	0.144	0.407	46	7
6729	1.285	5.147	0.250	0.685	30	2
4963	0.674	5.397	0.125	0.623	47	5
5512	0.537	3.208	0.167	0.439	44	6
6113	0.162	1.154	0.146	0.175	42	11
5544	0.200	2.658	0.075	0.368	46	10
6425	−0.049	0.674	0.072	−0.104	46	14
5797	0.132	2.343	0.056	0.327	49	12
6379	0.237	2.296	0.103	0.321	49	9
6376	0.319	5.493	0.058	0.638	47	8
4762	−0.138	1.387	0.100	−0.209	45	18
6613	0.056	1.915	0.029	0.277	49	13
6270	−0.053	0.745	0.071	−0.111	46	15
5780	−0.121	4.032	0.030	−0.511	49	17
6284	−0.360	7.039	0.051	−0.744	49	20
6203	−0.214	4.555	0.047	−0.562	49	19
5705	−0.085	1.164	0.073	−0.175	43	16

[a] See discussion in § 3.

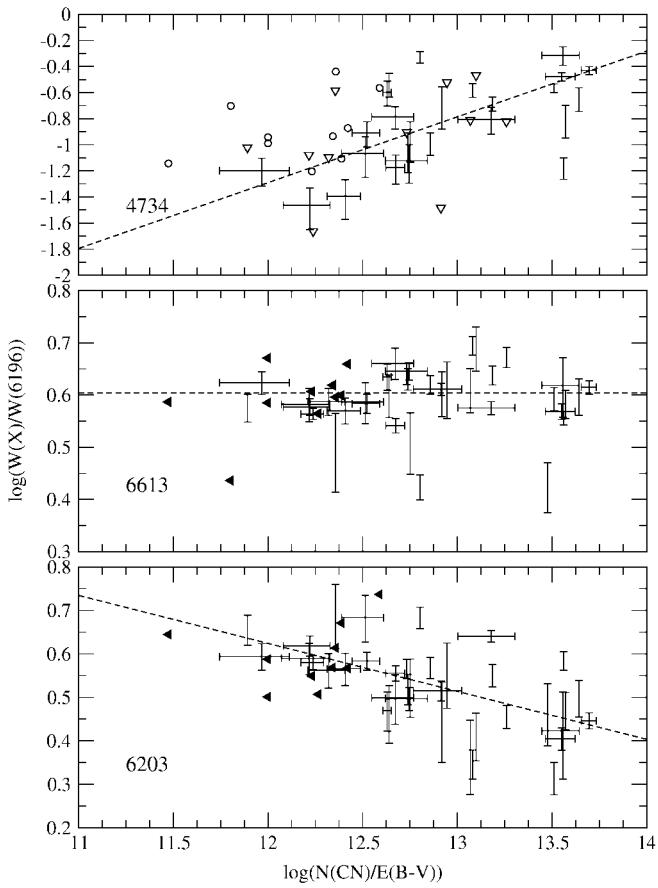

FIG. 5.—Same as Fig. 4*a*, but for normalized DIB equivalent widths vs. $N(\mathrm{CN})/E(B-V)$.

DIBs and CH (see Krełowski et al. 1999). In comparison with the results for C_2 and CN, three distinctive results follow from the data for CH.

1. The overall range in the values of N(CH) is smaller than the ranges in $N(C_2)$ and N(CN) by respective factors of about 4 and 6 in our particular, but representative, interstellar sample. The much smaller N(CH) baseline limits the accuracy with which the correlations of the DIBs with CH can be determined. Furthermore, for any particular pair of stars, the observed difference between the $W_\lambda(\mathrm{X})/W_\lambda(6196)$ ratios for any C_2 DIB therefore corresponds, on average, to a smaller, less easily detected difference in the CH abundance than in the corresponding abundances of C_2 and CN (see Table 3).

2. In sharp contrast to both C_2 and CN, the absolute strengths of nearly all bands in Table 2 correlate positively with N(CH), although generally with a large dispersion about the mean trend. As an important example, the data for λ6196 are presented in Figure 7.

3. For a typical C_2 DIB, the scatter about the respective fitting lines in plots of the normalized variables like those in Figures 4 and 5 is larger for CH than for either C_2 or CN.

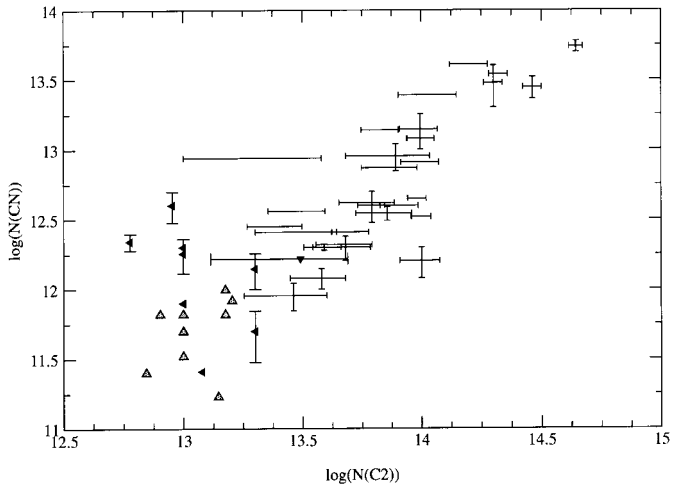

FIG. 6.—Log N(CN) vs. log $N(C_2)$. Large shaded triangles depict upper limits on both N(CN) and $N(C_2)$.

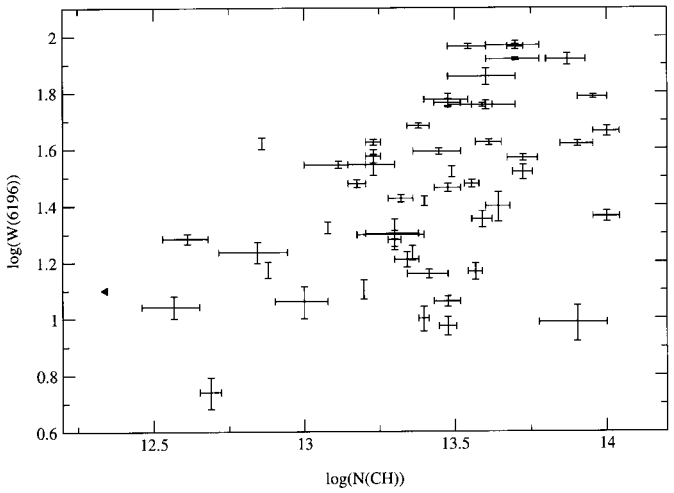

FIG. 7.—Log $W_\lambda(\lambda6196)$ vs. log N(CH)

In view of the second result just noted, the best choice of a normalizing DIB in the prospective comparisons with the CH abundances is less obvious. The use of λ6196 is desirable for continuity with C_2 and CN, although the statistically positive correlation of λ6196 with CH (Fig. 7) stands in marked contrast to the band's lack of correlation with C_2 and CN. Therefore, the *slope* of the relation between the basic variables W_λ(DIB) and N(CH) will be obscured in a plot of the corresponding normalized variables, although the scatter about the fitting line can still be determined as before. Ultimately, we again adopted λ6196 as the reference band for determining the relative DIB strengths. The qualitative difference between the CH slopes in the two kinds of correlation diagrams, based, respectively, on the unnormalized and the normalized variables, must therefore be carefully borne in mind, especially since this difference does not exist for the previous cases of C_2 and CN.

With this caveat, the values of the "CH slopes" are listed in the lower part of Table 4, and the three illustrative graphs in Figure 8 can be compared with those in Figures 4*a* and 5. For our observational sample, the relations between N(CH) and both $N(C_2)$ and N(CN) are shown in Figures 9 and 10, respectively. The disparity noted previously among the overall ranges in $N(C_2)$, N(CN), and N(CH) is evident in these figures.

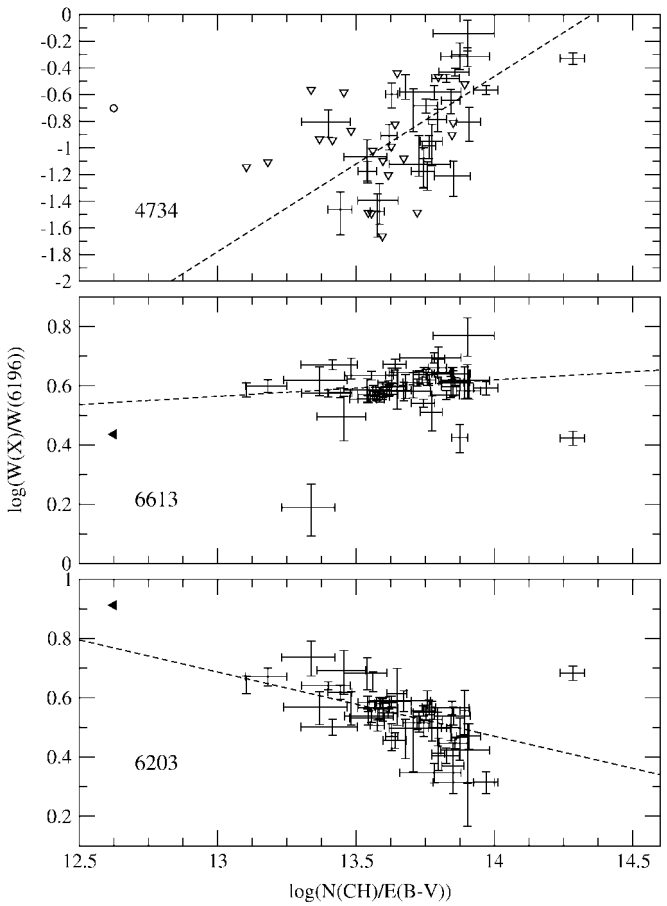

FIG. 8.—Same as Fig. 4*a*, but for normalized DIB equivalent widths vs. $N(\mathrm{CH})/E(B-V)$.

4.3. *Pairs of* C_2 *DIBs*

As seen in Figure 2, a conspicuous feature of the C_2 DIBs is that at least some are grouped into pairs with similar relative wavelength differences amounting to $\Delta\lambda/\lambda \approx 0.001$, or wavenumber differences $\Delta\sigma \approx \Delta\lambda/\lambda^2 \approx 20$ cm^{-1}. Five such pairs are listed in Table 5, where the agreement among the normalized splittings of the pairs located near 4966, 4982, and 5173 Å is especially good. A sixth pair, at 4726.27 and 4734.73 Å, exhibits crudely similar characteristics, $\Delta\lambda/\lambda = 0.0018$ and $\Delta\sigma = 38$ cm^{-1}; the precision of these values is limited somewhat by the blending of the short-wavelength member of the pair with a broader DIB centered near 4728.2 Å. (The latter band does not appear to be a C_2 DIB but incidentally yields corresponding splittings $\Delta\lambda/\lambda = 0.0014$ and $\Delta\sigma = 29$ cm^{-1}.) The remaining six, apparently unpaired C_2 DIBs listed in Table 2, such as λ4363 and λ5512, could have similarly paired partners that are obscured by blending or that are too weak to be detected in our spectra, or both. The relative strengths of the short-wavelength and long-wavelength members in each of the five pairs of C_2 DIBs in Table 5 do not show a fixed pattern (Fig. 2).

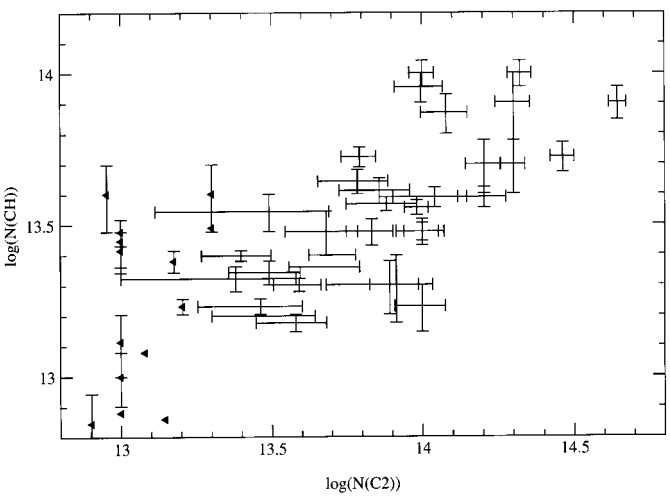

FIG. 9.—Log $N(\mathrm{CH})$ vs. log $N(C_2)$

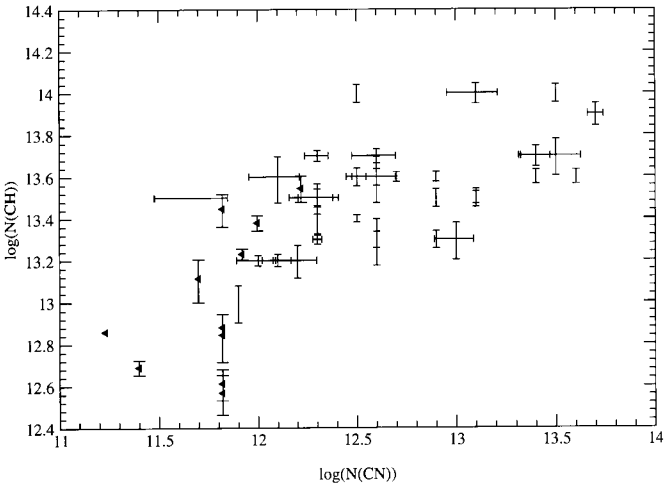

FIG. 10.—Log $N(\mathrm{CH})$ vs. log $N(\mathrm{CN})$

Although these data do not suggest to us an identification with a specific molecular absorber, the splittings are reminiscent of a spin-orbit interaction in a linear molecule (Herzberg 1991). In that case, at least some of the respectively summed pairs of band strengths might show a tighter correlation with each other than does either of the individual lines of one pair with either of those of another. As a test of this possibility, we found that a plot of the sum $W_\lambda(4979) + W_\lambda(4984)$ versus the sum $W_\lambda(4963) + W_\lambda(4969)$ does show a well-defined relation. However, the scatter of these data points about the fitting curve is statistically comparable to that in a plot of $W_\lambda(4979)$ versus $W_\lambda(4963)$, for example, or to that in similar plots of any of the other three pairs of individual band strengths. Therefore, this test is currently inconclusive with respect to the hypothesis of a spin-orbit interaction.

TABLE 5
C_2 DIB SPLITTINGS

C_2 DIB (Å)	C_2 DIB (Å)	$\Delta\lambda$ (Å)	$1000 \times \Delta\lambda/\lambda$	$\Delta\sigma$ (cm^{-1})
4963.96	4969.12	5.16	1.04	20.9
4979.58	4984.73	5.15	1.03	20.7
5170.44	5175.99	5.55	1.07	20.7
5541.77	5546.46	4.69	0.85	15.3
5762.74	5769.08	6.34	1.10	19.1

5. SUMMARY

The spectra acquired in our survey will eventually provide new observational data for most of the known DIBs, with an advantageous combination of broad wavelength coverage, relatively high resolution, and a high S/N that can be achieved in feasibly short total observing times. Separate, future papers are planned in this series to describe not only additional observational results from the survey but also fuller interpretations of the empirical results presented here.

In this paper, 21 selected DIBs are measured and analyzed in the spectra of 53 stars with $0.11 \leq E(B-V) \leq 1.99$. In these 53 directions, the normalized strengths, $W_\lambda(\mathrm{X})/W_\lambda(\lambda 6196)$, of seven narrow, weak "C_2 DIBs" among this group correlate well with $N(C_2)/E(B-V)$, the average abundance of C_2, via power laws. In contrast, the similarly normalized equivalent widths of the other 14 DIBs are uncorrelated, or weakly anticorrelated, with $N(C_2)/E(B-V)$. The polyatomic molecule(s) presumed to cause these seven C_2 DIBs may therefore bear a direct chemical relation to interstellar C_2 molecules that is not shared by the molecules that are assumed to give rise to the other 14 well-known DIBs. The $\lambda 4963$ band is generally the strongest of these C_2 DIBs, while the $\lambda 4734$ band shows the most sensitive correlation with $N(C_2)/E(B-V)$. Eleven other C_2 DIBs are also identified but are not analyzed here. The very close correlation between $N(C_2)$ and $N(C_3)$ discovered by Oka et al. (2003) further extends this connection to interstellar C_3 molecules as well.

The normalized strengths of the seven C_2 DIBs also show positive correlations with the average abundances of both CN and CH, in our sample of light paths. The relative strengths of these bands prove to depend more sensitively on $N(C_2)/E(B-V)$ than on $N(\mathrm{CN})/E(B-V)$, and the scatter in the correlation with the C_2 DIBs is larger for CH than for C_2 (and CN). Because the range of $N(\mathrm{CH})$ over the 53 light paths investigated here is smaller than the corresponding ranges of $N(C_2)$ and $N(\mathrm{CN})$ by appreciable factors, the correlations with C_2 and CN are also more easily detected observationally than that with CH, and they are better defined by the larger column-density baselines provided by C_2 and CN. While the strengths of the 14 other DIBs also investigated here are uncorrelated, or weakly anticorrelated, with $N(C_2)/E(B-V)$ and $N(\mathrm{CN})/E(B-V)$, most correlate positively with $N(\mathrm{CH})/E(B-V)$.

This work is based on observations obtained with the Apache Point Observatory 3.5 m telescope, which is owned and operated by the Astrophysical Research Consortium. We are grateful to the referee for valuable suggestions that have improved this paper. B. J. M. has been supported by the Miller Institute for Basic Research in Science, University of California at Berkeley. T. O. acknowledges support from NSF grants PHY-9722691 and PHY-0099442. S. D. F. and P. S. are supported by NASA Contract NAS5-32985 to Johns Hopkins University. Subcontracts from that same contract, to the University of Colorado and the University of Chicago, provided support to T. P. S. and D. G. Y., respectively. D. E. W. acknowledges support from NASA LTSA grant NAG5-3228.

APPENDIX

Tables 6A and 6B collect the measured equivalent widths of the 21 DIBs analyzed in this paper, along with the derived interstellar column densities of C_2, CN, and CH, for each of 53 stars. A few comments about the column densities may be useful, although a fuller explanation of these results is planned for a future paper.

All of the values of $N(C_2)$ have been derived from our own spectra, by methods outlined below. In contrast, for roughly half of the stars in Tables 6A and 6B, the values of $N(\mathrm{CN})$ and/or $N(\mathrm{CH})$ were taken from the literature, when results based on spectra obtained at higher resolution (but generally lower S/N) are available. In some of these cases, the entries in the table reflect the fact that no estimates of the uncertainties were provided. Many of these earlier results have already been tabulated by various authors (Federman et al. 1994; Crane, Lambert, & Sheffer 1995; Welty & Hobbs 2001), along with references to the original papers. In the cases for which values of $N(\mathrm{CN})$ and/or $N(\mathrm{CH})$ were not available from the literature, these values were derived in the optically thin limit from equivalent widths measured in our spectra, at $W_\lambda \leq 15$ mÅ. Slightly stronger lines of CH were unavoidably used in a few cases.

For CH, the smaller column densities were based on the $\lambda 4300$ line, while some of the larger values were derived from one or more of the three intrinsically weaker lines near $\lambda 3886$, in order to minimize the effects of line saturation. The weaker $\lambda 3878$ and $\lambda 3890$ lines arise from the lower λ-doubled level. When these two lines were not detected, the population of that level was assumed equal to that of the upper λ-doubled level, from which the stronger $\lambda 3886$ line arises. Similarly, for CN, the lower column densities were based on one or more of the lines near $\lambda 3875$, but some of the higher values followed from the lines of the multiplet near $\lambda 7906$. A population ratio $N(J=0)/N(J=1) = 2$ was assumed if lines arising only from the $J=0$ level were detectable. In cases for which lines from both the $J=0$ and the $J=1$ levels were measurable but not appreciably saturated, the observed population ratios ranged from about 1.5 to 2.5.

The column densities $N(C_2)$ are frequently more difficult to estimate accurately. The lines of the (2–0) Phillips band at $8750 < \lambda < 8818$ Å are usually best suited for a determination of $N(C_2)$ from our spectra. With bandheads near 10133 and 7714 Å, respectively, the (1–0) and (3–0) bands are also present and were additionally used in the analyses for a few stars. For C_2, the primary difficulty arises from the substantial number of excited rotational levels, typically with $J > 8$, whose collective population should not be neglected, although the populations of these individual levels are, respectively, too small to be observed directly. Fortunately, the relative populations of all rotational levels up to $J = 24$ have been measured in UV spectra of ζ Oph by Lambert, Sheffer, & Federman (1995) and also of most or all levels up to $J = 20$ in our spectra of Cyg OB2 5, Cyg OB2 12, and HD 204827. From the data for these four stars, we derived an "average" set of relative level populations for $J \leq 20$, without regard for the differences in physical conditions in the four distinct sets of interstellar clouds. For $10 \leq J \leq 20$, the average distribution varies approximately as $J^{-1.6}$. For all of our program stars, this fixed distribution was

TABLE 6A

MEASUREMENTS FOR PROGRAM STARS

Star	4734[a] (mÅ)	4762 (mÅ)	4963[a] (mÅ)	4984[a] (mÅ)	5175[a] (mÅ)	5512[a] (mÅ)	5544 (mÅ)	5705 (mÅ)	5769[a] (mÅ)	5780 (mÅ)	5797 (mÅ)	6113 (mÅ)
20041	4.3 ± 1.4	46 ± 8	18.3 ± 1.2	7.3 ± 2	9 ± 3	6 ± 1	20 ± 5	101 ± 7	<3.5	439 ± 8	161 ± 6	30.2 ± 1.5
21483	5.1 ± 1	29 ± 5	18 ± 1	11.3 ± 1	11.4 ± 1	5.3 ± 1	12.7 ± 1	35 ± 10	5.6 ± 1.5	181 ± 7	96 ± 6	8.3 ± 1
21389	<3	57 ± 6	11 ± 1.5	14 ± 4	<2.5	4.9 ± 0.7	38.6 ± 1	104 ± 7	<3	411 ± 8	160 ± 7	20 ± 1.5
23180	2.6 ± 0.9	19 ± 6	15.7 ± 1.5	6.4 ± 1	20.3 ± 1.5	8.6 ± 0.8	9.9 ± 1	45 ± 6	5.2 ± 1	101 ± 7	81.6 ± 6	4.5 ± 0.9
281159	5.4 ± 1	26 ± 5	23 ± 1	13.3 ± 1	12.6 ± 1.5	12.3 ± 1	17.8 ± 1	68 ± 10	5.3 ± 1	310 ± 10	120 ± 15	19 ± 2
24398	<2.5	26 ± 8	8.8 ± 1	5.9 ± 1	15.3 ± 1	4.9 ± 1	6.8 ± 1.2	36 ± 10	<3	114 ± 7	77 ± 5	7.4 ± 1
24534	<5	45 ± 7	13.8 ± 1	10.6 ± 1	7.2 ± 1	5.9 ± 0.8	6.9 ± 1	<30	8.5 ± 2	98 ± 8	68 ± 4	8.7 ± 1
24912	<2	31 ± 4	8.4 ± 1	3.2 ± 0.5	<2.5	3.1 ± 0.8	8.3 ± 1	24 ± 7	2.6 ± 0.9	209 ± 7	46 ± 7	3.2 ± 1
26571	9.7 ± 1	<15	22 ± 2	16 ± 3	11.8 ± 2	12.5 ± 1.5	12.4 ± 4	48 ± 7	6.1 ± 1.5	151 ± 7	82.6 ± 10	10.1 ± 1.5
27778	1.8 ± 0.5	<10	9 ± 1	4 ± 1	3.9 ± 0.6	3 ± 1	7.5 ± 1	17 ± 3	<2	86 ± 4	39 ± 2	4.5 ± 1
29647	7 ± 1.5	<35	14.3 ± 1	3.4 ± 1.2	8.3 ± 1.5	7.2 ± 1.3	<5	<24	4.6 ± 1.5	70 ± 7	39 ± 5	11 ± 2.5
30614	<2	17 ± 3	3.5 ± 0.8	3.4 ± 1	<3	<2	9.4 ± 1	54 ± 10	<3	133 ± 5	56 ± 3	6.4 ± 1
34078	10.8 ± 1	64 ± 3	27 ± 2	7.5 ± 1	14.7 ± 1	4.5 ± 1	13 ± 2	48 ± 3	2.6 ± 0.8	181 ± 5	56 ± 3	12 ± 1
35149	<2	<18	2.2 ± 0.7	<2.5	<2	<3	<2.5	<12	<2	57 ± 3	15.7 ± 3	<3
36371	<3	63 ± 7	21.6 ± 2	6.4 ± 1	4.3 ± 1	5.6 ± 1	15 ± 1	72 ± 5	<3	313 ± 7	127 ± 7	20.6 ± 2
37061	<2.5	<25	<2.5	<2.5	<2	<4	3.5 ± 1	46 ± 5	<2.5	169 ± 7	35 ± 5	<2.5
37903	<3	31 ± 7	<5	<3	<3	<2	4.1 ± 1	36 ± 5	<3	183 ± 10	33 ± 5	<3
41117	1.4 ± 0.5	51 ± 3	20 ± 1	9 ± 1	8.7 ± 1	9 ± 1	16 ± 1	86 ± 5	<2.5	356 ± 10	148 ± 8	16 ± 1.5
42087	3.7 ± 0.8	50 ± 2	23 ± 2	7.5 ± 1	8.5 ± 1	9 ± 1	16 ± 2	75 ± 6	3.9 ± 0.8	275 ± 7	99 ± 2	18 ± 3
43384	<3	65 ± 3	22 ± 2	6.5 ± 1	2.6 ± 0.8	7 ± 1	26 ± 1	113 ± 4	<3	455 ± 7	155 ± 5	20 ± 1
46202	3 ± 1	60 ± 6	21 ± 3	6.5 ± 1	8.4 ± 1.5	9 ± 1	18.7 ± 1.5	76 ± 10	<5	337 ± 8	145 ± 9	18 ± 2
46711	5.1 ± 1.5	109 ± 10	32 ± 2	21 ± 2	13.3 ± 1.5	17 ± 2	45 ± 2	173 ± 15	9.8 ± 1.5	820 ± 10	269 ± 8	31 ± 2
48099	<1.5	35 ± 5	7.4 ± 1	2.8 ± 0.9	<2	<1.5	7.3 ± 1	43 ± 5	<2	207 ± 7	58 ± 5	8.3 ± 1
50064	<6	126 ± 10	32 ± 3	14.5 ± 2.5	4.7 ± 1.5	18 ± 2	38 ± 5	154 ± 12	<6	693 ± 10	288 ± 15	29 ± 4
53367	2.8 ± 0.9	57 ± 6	16 ± 2	5.6 ± 1	18.7 ± 2	5.5 ± 1	9.6 ± 1.2	40 ± 6	2.5 ± 0.8	177 ± 9	82 ± 8	11.2 ± 1.5
147888	4.8 ± 1	14 ± 3	18 ± 2	11 ± 1	6 ± 1	12 ± 1	6 ± 1	54 ± 4	7.6 ± 1	252 ± 12	60 ± 5	5.5 ± 1
147889	12.5 ± 0.8	46 ± 4	55 ± 2	25 ± 1	25 ± 1	19 ± 1	22 ± 1	97 ± 4	17.5 ± 1.5	377 ± 8	163 ± 5	16 ± 1
147933	5 ± 1	19.5 ± 5	23.2 ± 1	10.3 ± 0.8	7.8 ± 1	15 ± 1	6.4 ± 1	44 ± 8	10.4 ± 1.5	222 ± 10	71 ± 6	3.5 ± 1
149757	<3	15 ± 2	6 ± 1	4.6 ± 0.6	2.8 ± 0.6	2.9 ± 0.8	4.1 ± 0.6	<18	<3	83 ± 7	38 ± 4	3.3 ± 0.6
166734	<3	85 ± 5	33 ± 1	14.5 ± 1	10.7 ± 1	25 ± 2	54 ± 1.5	168 ± 9	7 ± 2	727 ± 8	322 ± 15	48.6 ± 2
167971	2 ± 0.7	67 ± 6	23 ± 1	14 ± 1	5.1 ± 0.8	10 ± 1	25 ± 2	131 ± 5	<5	512 ± 9	208 ± 6	19 ± 2
168076	2.4 ± 0.8	98 ± 6	27.5 ± 1.5	15 ± 2	4.7 ± 1.5	15 ± 2	33 ± 1.5	118 ± 12	6 ± 2	541 ± 10	250 ± 8	27 ± 4
169454	3.8 ± 0.7	91 ± 6	26 ± 1	14 ± 1	23 ± 1	14 ± 1	26 ± 1	118 ± 5	6.5 ± 1	510 ± 7	213 ± 5	18 ± 1
170740	<4	17 ± 4	11 ± 2	5.8 ± 0.8	10.4 ± 1.2	6.7 ± 0.7	9.8 ± 0.7	63 ± 5	<6	255 ± 7	92 ± 5	10.3 ± 0.8
172028	12.3 ± 0.8	38 ± 4	50 ± 1	26 ± 1	23 ± 2	26 ± 1	26 ± 1	53 ± 5	17 ± 1.5	256 ± 8	217 ± 5	20 ± 1
179406	5.2 ± 0.6	15 ± 2	20 ± 1	12.3 ± 1	10.5 ± 0.6	11 ± 1	9 ± 1	29 ± 6	7.1 ± 0.6	172 ± 5	76 ± 3	9 ± 1
183143	<2	122 ± 7	26 ± 1	14 ± 1	2.2 ± 0.7	11 ± 1	32 ± 2	172 ± 7	<3	758 ± 8	295 ± 10	39 ± 2
185418	<4	18 ± 2	10 ± 1	3.3 ± 0.8	3.5 ± 0.8	3.2 ± 0.8	14 ± 1	57 ± 3	3.8 ± 0.7	273 ± 5	105 ± 5	14.3 ± 0.8
186994	<3	24 ± 6	<3	<3	<3	<4	<3	<30	<3	101 ± 5	23 ± 4	<4
192639	<4	44 ± 4	9 ± 1	6.7 ± 1	<2	4.5 ± 0.8	14 ± 1	81 ± 5	<4	324 ± 5	79 ± 7	11.5 ± 1
229059	<2	62 ± 6	31 ± 2	12 ± 2	10 ± 1.2	12 ± 1	40 ± 2	96 ± 5	4.7 ± 1.3	457 ± 7	163 ± 3	25 ± 2
Cyg OB2 5	13 ± 3	93 ± 7	51 ± 2	20 ± 2	19 ± 2	15 ± 1	45 ± 3	195 ± 20	7.4 ± 1.5	774 ± 8	239 ± 12	32 ± 4
198478	2.1 ± 0.5	46 ± 3	11.5 ± 1	6.7 ± 0.8	6.4 ± 1	6.5 ± 1	10 ± 1	72 ± 4	<2	332 ± 5	112 ± 4	12.3 ± 1
199579	<1.8	25 ± 2	10 ± 1	4 ± 1	2.8 ± 0.7	3.8 ± 1	7 ± 1	21 ± 3	<2.5	126 ± 3	54 ± 4	4.2 ± 1
203938	2.8 ± 0.7	46 ± 3	24 ± 1	8.3 ± 1	9.1 ± 1.5	9.3 ± 1	17.4 ± 1	68 ± 4	<3.5	356 ± 5	152 ± 5	14 ± 1.5
204827	15.4 ± 1	49 ± 2	55 ± 1	30.4 ± 0.9	37.4 ± 1	23 ± 1	29.4 ± 1	58 ± 3	19.3 ± 1	257 ± 4	199 ± 3	23.6 ± 1.2
206165	2.4 ± 0.8	51 ± 5	15.8 ± 1	8.4 ± 1	8.8 ± 1	7.3 ± 0.7	10.8 ± 1	58 ± 5	6.6 ± 1.5	231 ± 7	106 ± 5	11 ± 1
206267	6 ± 0.7	42 ± 3	24 ± 2	11.5 ± 1	8.6 ± 1	10 ± 1	12 ± 1	59 ± 4	4.6 ± 1	242 ± 7	102 ± 5	13 ± 1
207198	3.1 ± 0.6	54 ± 3	29 ± 1	15 ± 1	9.9 ± 1	18 ± 1	24.3 ± 1	56 ± 5	6 ± 1	262 ± 6	144 ± 3	13 ± 1
210121	4.7 ± 1	16.4 ± 3	11 ± 1	7.4 ± 1	6.2 ± 1	3.7 ± 1	8 ± 1	<20	2.9 ± 0.9	70 ± 7	46 ± 9	2.2 ± 0.7
210839	<4	31 ± 3	11 ± 1	5.2 ± 1	3.1 ± 0.8	7.5 ± 1	12.6 ± 0.8	65 ± 5	<3	261 ± 5	72 ± 6	16 ± 1
218376	<2	13 ± 2	6.3 ± 0.6	3.3 ± 0.6	<4	5.2 ± 1	4.4 ± 1	45 ± 5	<3	146 ± 8	61.7 ± 6	7.1 ± 1.5
BD+63 1964	<3	122 ± 7	36 ± 1	19 ± 1	7.5 ± 1.5	25 ± 1	46 ± 2	211 ± 20	<4	729 ± 10	419 ± 12	41 ± 2

[a] C_2 DIB.

TABLE 6B

MEASUREMENTS FOR PROGRAM STARS

Star	6196 (mÅ)	6203 (mÅ)	6270 (mÅ)	6284 (mÅ)	6376 (mÅ)	6379 (mÅ)	6425 (mÅ)	6613 (mÅ)	6729[a] (mÅ)	$N(C_2)$ (1e12)	N(CH) (1e12)	N(CN) (1e12)
20041	57 ± 2	179 ± 9	165 ± 7	1030 ± 60	50 ± 2	86 ± 1	19.6 ± 1	252 ± 4	<3.5	<9	40 ± 10	4 ± 1
21483	22.5 ± 1.5	71 ± 5	59 ± 8	397 ± 45	23 ± 2	51.5 ± 1	8 ± 1.5	89 ± 4	4.1 ± 0.8	110 ± 30	39 ± 3	24.5 ±
21389	41.7 ± 2	184 ± 9	102 ± 10	1211 ± 80	26 ± 2.5	44 ± 1.5	15 ± 1.5	161 ± 4	<2	<14	7 ±	<0.2
23180	12.7 ± 1	36 ± 7	21 ± 7	200 ± 60	9.8 ± 1.5	45.6 ± 1	4 ± 1.4	51 ± 3	4.7 ± 0.8	32 ± 12	16 ±	2.6 ±
281159	33 ± 2	104 ± 12	73 ± 6	635 ± 80	30.7 ± 1.5	61 ± 2	7.6 ± 1.5	151 ± 5	5 ± 1	62 ± 8	53 ± 4	4 ± 1
24398	16.2 ± 1	38 ± 7	<20	185 ± 50	16.4 ± 2.5	67 ± 3	6.3 ± 1.5	66 ± 5	3.2 ± 0.9	31 ± 8	22 ± 2	3.6 ±
24534	14.7 ± 1	38 ± 4	21 ± 4	270 ± 60	18 ± 4	40.5 ± 1	7.2 ± 1.5	72 ± 5	4.6 ± 1.2	76 ± 20	37 ± 2	7.4 ±
24912	21 ± 1	95 ± 6	49 ± 5	507 ± 60	13 ± 1.5	30.4 ± 1	5 ± 1	79 ± 3	<2.5	<12	12 ±	0.3 ±
26571	20 ± 2.5	53 ± 10	35.5 ± 5	273 ± 40	20 ± 4	50.6 ± 1.5	8 ± 2.5	83 ± 3	3.3 ± 1	78 ± 30	20 ± 4	9 ± 2
27778	11.5 ± 0.5	34 ± 3	<10	170 ± 50	7.5 ± 1	20 ± 1	3.5 ± 1	44 ± 2	3.4 ± 0.7	68 ± 12	30 ± 3	13.8 ±
29647	9.7 ± 1.4	20 ± 5	14.6 ± 4	95 ± 25	11.4 ± 2	18.5 ± 1	7.6 ± 1.2	57 ± 2	2.7 ± 0.9	200 ± 26	80 ± 20	>120
30614	17.2 ± 1.5	63.7 ± 6	49 ± 6	360 ± 60	14 ± 1.5	34.5 ± 1	4.9 ± 0.7	71.5 ± 5	<3	<8	7 ± 1.8	<0.7
34078	23 ± 1	111 ± 4	56 ± 3	510 ± 80	9 ± 1	18 ± 1	5 ± 1	61 ± 2	<3	100 ± 9	100 ± 10	3.3 ±
35149	5.5 ± 0.7	22.6 ± 4	11.5 ± 2.5	286 ± 45	<4	6.1 ± 1	3.9 ± 1.2	21.7 ± 2	<2.5	<7	5 ± 0.4	<0.3
36371	37.5 ± 2	137 ± 10	75 ± 5	743 ± 60	30 ± 3	79 ± 1.5	15.5 ± 1	145 ± 4	<2.5	29 ± 11	17 ± 1	0.9 ± 0.2
37061	12.6 ± 1.5	103 ± 6	30.5 ± 6	675 ± 55	7.1 ± 2	7.2 ± 1.5	<5	34.4 ± 3	<2.5	<10	<2.2	<0.3
37903	11.5 ± 1.5	56.6 ± 6	19 ± 5	503 ± 70	<4	3.5 ± 1	4.3 ± 1	36 ± 4	<3	<10	10 ± 2	0.8 ±
41117	42 ± 1	135 ± 5	108 ± 4	760 ± 100	29 ± 1	136 ± 5	13 ± 1	154 ± 3	1.8 ± 0.6	<16	17 ± 1	<0.8
42087	30 ± 1	115 ± 4	64 ± 4	675 ± 70	23 ± 4	68 ± 3	10 ± 1.5	115 ± 3	3.5 ± 0.7	38 ± 10	15 ± 1	1.2 ± 0.2
43384	48 ± 1	170 ± 6	120 ± 3	950 ± 50	36 ± 2	90 ± 2	16 ± 1	194 ± 3	<3	<15	24 ± 2	<1
46202	35 ± 3	169 ± 15	84 ± 5	850 ± 100	27 ± 3	56 ± 2	10 ± 1.5	135 ± 4	<3	100 ± 19	17 ± 3	1.6 ± 0.4
46711	83 ± 4	287 ± 14	197 ± 15	1500 ± 150	73 ± 4	170 ± 5	24.3 ± 1.5	363 ± 5	8.2 ± 1.5	120 ± 21	74 ± 11	...
48099	19.2 ± 0.8	90 ± 5	45 ± 4	578 ± 50	12.8 ± 1.5	19.8 ± 0.8	7.3 ± 0.8	76.3 ± 2	<2	<15	4 ± 0.7	<0.7
50064	72 ± 5	280 ± 12	178 ± 15	1415 ± 150	57 ± 4	146 ± 4	24 ± 2	275 ± 6	<6	<20	40 ± 10	1.4 ± 0.4
53367	25 ± 3	84 ± 8	28 ± 6	565 ± 70	28 ± 3	29 ± 2	5.1 ± 1.5	81 ± 5	5.4 ± 1	61 ± 16	44 ± 4	4.2 ±
147888	19 ± 1	56 ± 5	72 ± 3	390 ± 60	21 ± 1	33 ± 1	3 ± 1	82 ± 2	2.3 ± 0.7	39 ± 7	20 ± 1	2 ± 0.1
147889	46 ± 2	95 ± 7	56 ± 3	530 ± 50	64 ± 2	93 ± 2	7.5 ± 1	180 ± 5	17.5 ± 1	210 ± 19	100 ± 10	34.7 ±
147933	17.1 ± 1	50 ± 7	30 ± 5	426 ± 80	17.3 ± 2	28 ± 1	3 ± 1	68 ± 5	2.7 ± 0.9	49 ± 13	23 ±	2.1 ±
149757	10 ± 1	36 ± 5	<15	175 ± 35	12.5 ± 1	20 ± 1	<3	41 ± 3	<2	25 ± 7	25 ± 1	2.8 ±
166734	93 ± 3	321 ± 12	243 ± 10	1560 ± 200	94 ± 3	229 ± 7	30.5 ± 1.5	401 ± 5	11.5 ± 2	160 ± 21	50 ± 10	...
167971	58 ± 2	241 ± 10	145 ± 8	1450 ± 200	39 ± 2	85 ± 2	17 ± 1	219 ± 3	2.6 ± 0.8	<10	30 ± 3	1.8 ± 0.5
168076	59.5 ± 3	219 ± 15	128 ± 10	1090 ± 150	43 ± 3	108 ± 4	12.3 ± 1.5	221 ± 6	3.8 ± 1	48 ± 13	30 ± 5	2 ± 0.4
169454	57 ± 1	219 ± 10	90 ± 4	1580 ± 170	41 ± 2	142 ± 3	12 ± 1	205 ± 5	7 ± 1.5	160 ± 29	39 ± 3	40.7 ±
170740	26.6 ± 0.8	76 ± 4	70 ± 6	595 ± 60	21.6 ± 1	64.5 ± 1	9.7 ± 0.8	125 ± 4	4.8 ± 1.5	24 ± 14	21 ± 2	8.7 ±
172028	37 ± 1	94 ± 5	45 ± 5	450 ± 60	42 ± 3	96 ± 2	13 ± 1	137 ± 3	10.5 ± 1	290 ± 26	53 ± 6	28 ± 5
179406	19.8 ± 0.7	44 ± 3	33 ± 4	430 ± 60	20 ± 2	58 ± 2	8 ± 1	98 ± 2	5.2 ± 0.8	82 ± 15	20 ± 5	4 ±
183143	92 ± 2	350 ± 11	268 ± 10	1930 ± 150	58 ± 2	113 ± 3	26 ± 1	337 ± 4	9 ± 3	<6	50 ± 3	2.2 ± 0.3
185418	35 ± 1	111 ± 6	108 ± 5	640 ± 50	29 ± 2	71 ± 2	14 ± 1	164 ± 4	<2.5	<10	13 ± 3	<0.5
186994	11 ± 1	60 ± 6	17 ± 5	296 ± 40	7.5 ± 2.5	5.6 ± 1.5	<5	17 ± 3	<2	<10	4 ± 0.8	<0.7
192639	39 ± 1	151 ± 5	72 ± 5	817 ± 50	24.6 ± 2	42 ± 2	11.5 ± 1	150 ± 3	<4	<10	28 ± 5	<0.7
229059	61 ± 1	200 ± 10	122 ± 5	1090 ± 150	51 ± 2	65 ± 2	17 ± 2	249 ± 5	4 ± 1	99 ± 18	90 ± 10	14 ± 4
Cyg OB2 5	83 ± 1	363 ± 10	205 ± 15	1990 ± 200	63 ± 4	95 ± 2	27 ± 2	312 ± 8	5.8 ± 1.5	200 ± 18	50 ± 10	30 ± 10
198478	33.1 ± 1.5	130 ± 7	94 ± 7	919 ± 60	22.6 ± 1.5	102 ± 1.5	16.3 ± 1.5	139 ± 3	<3	<20	31 ±	0.5 ± 0.2
199579	14.4 ± 0.5	53 ± 2	28 ± 4	315 ± 50	14.5 ± 1	19 ± 2	5 ± 1.5	63 ± 2	<1.5	<10	26 ± 4	2 ±
203938	42 ± 1	151 ± 5	82 ± 4	936 ± 60	29 ± 2	54 ± 1	13 ± 2	146 ± 3	3.3 ± 1	72 ± 19	41 ± 4	3.5 ± 0.4
204827	41.5 ± 1	116 ± 4	82 ± 5	518 ± 60	45 ± 2	96 ± 1.5	16 ± 0.8	171 ± 3	17 ± 1.2	440 ± 29	80 ± 10	55 ± 5
206165	26 ± 1	86 ± 6	57 ± 5	486 ± 60	23.2 ± 1.5	71.8 ± 2	11.4 ± 2	111 ± 3	2 ± 0.6	51 ± 9	25 ±	2.6 ±
206267	29 ± 1	103 ± 5	74 ± 3	544 ± 45	23 ± 2	40 ± 2	14 ± 1	126 ± 3	2.9 ± 0.6	100 ± 18	30 ± 3	8.1 ±
207198	30 ± 1	111 ± 5	58 ± 3	543 ± 40	35 ± 2	75 ± 2	14 ± 1	125 ± 3	6.4 ± 0.8	96 ± 9	36 ± 2	4.5 ±
210121	9.4 ± 0.7	27.5 ± 4	6 ± 2	146 ± 50	3.9 ± 1	15.5 ± 1	<7	25 ± 2	2 ± 0.7	100 ± 13	30 ± 2	12 ±
210839	31 ± 1	106 ± 5	69 ± 3	551 ± 45	28 ± 2	58 ± 2	14.7 ± 1	150 ± 3	2.2 ± 0.7	50 ± 19	...	3.7 ±
218376	14.9 ± 1	55 ± 6	33.6 ± 5	365 ± 45	12 ± 2	40.5 ± 2	8.1 ± 1	68 ± 3	<2.5	<10	8 ±	<0.7
BD+63 1964	92 ± 2	313 ± 15	135 ± 4	1380 ± 200	75 ± 3	175 ± 3	22 ± 1	330 ± 6	11.5 ± 1.5	31 ± 18	35 ± 5	<1.7

[a] C_2 DIB.

used to estimate crudely the unobserved populations of all levels from $J = J_{max} + 2$ through $J = 20$, where J_{max} identifies the most highly excited level whose population was observed directly. For a typical program star with $J_{max} = 8$, the resulting ratio of the sum of the unobserved populations at $J > J_{max}$ to the sum of those observed at $J \leq J_{max}$ was about 0.15. Although systematic, these extrapolative corrections thus proved to be generally small. For stars for which only upper limits on $N(C_2)$ are available, the observed upper limit on $N(J = 2)$ was used to set the absolute scale for $N(C_2)$.

In contrast to the case of the high-resolution measurements often available for CN and CH from the literature, the narrow C_2 lines are usually unresolved in our spectra. Therefore, crude corrections for line saturation were also incorporated uniformly into all values of $N(C_2)$ in Table 6B, by deriving the column densities from the curve of growth for a single Gaussian line component with a line-width parameter $b = 0.75$ km s^{-1}. Except for a few stars with relatively strong C_2 absorption, these saturation corrections to the optically thin column densities were still smaller than the corrections for the unobserved populations of the excited rotational levels.

REFERENCES

Blaauw, A. 1963, in Basic Astronomical Data, ed. K. A. Strand (Chicago: Univ. Chicago Press), 401
Bohlin, R. C., Savage, B. D., & Drake, J. F. 1978, ApJ, 224, 132
Crane, P., Lambert, D. L., & Sheffer, Y. 1995, ApJS, 99, 107
Federman, S. R., Strom, C. J., Lambert, D. L., Cardelli, J. A., Smith, V. V., & Joseph, C. L. 1994, ApJ, 424, 772
Galazutdinov, G. A., Musaev, F. A., Krełowski, J., & Walker, G. A. H. 2000, PASP, 112, 648
Herbig, G. H. 1967, in IAU Symp. 31, Radio Astronomy and the Galactic System, ed. H. van Woerden (San Francisco: ASP), 85
———. 1975, ApJ, 196, 129
———. 1995, ARA&A, 33, 19
Herzberg, G. 1991, Molecular Spectra and Molecular Structure, Vol. III: Electronic Spectra and Electronic Structure of Polyatomic Molecules (Malabar: Krieger), 54
Jenniskens, P., & Désert, F.-X. 1993, A&A, 274, 465
———. 1994, A&AS, 106, 39
Johnson, H. L. 1963, in Basic Astronomical Data, ed. K. A. Strand (Chicago: Univ. Chicago Press), 214
Krełowski, J., Ehrenfreund, P., Foing, B. H., Snow, T. P., Weselak, T., Tuairisg, S. Ó., Galazutdinov, G. A., & Musaev, F. A. 1999, A&A, 347, 235
Krełowski, J., & Sneden, C. 1993, PASP, 105, 1141
Krełowski, J., Sneden, C., & Hiltgen, D. 1995, Planet. Space Sci., 43, 1195
Lambert, D. L., Sheffer, Y., & Federman, S. R. 1995, ApJ, 438, 740
Leitherer, C., et al. 2001, STIS Instrument Handbook, Vol. 5.1 (Baltimore: STScI)
McCall, B. J., Oka, T., Thorburn, J., Hobbs, L. M., & York, D. G. 2002, ApJ, 567, L145
McCall, B. J., Thorburn, J., Hobbs, L. M., Oka, T., & York, D. G. 2001, ApJ, 559, L49
Merrill, P. W. 1934, PASP, 46, 206
Oka, T., Thorburn, J. A., McCall, B. J., Friedman, S. D., Hobbs, L. M., Sonnentrucker, P., Welty, D. E., & York, D. G. 2003, ApJ, 582, 823
Rousseeuw, P. J., & Leroy, A. M. 1987, Robust Regression and Outlier Detection (New York: Wiley)
Snow, T. P., Welty, D. E., Thorburn, J., Hobbs, L. M., McCall, B. J., Sonnentrucker, P., & York, D. G. 2002, ApJ, 573, 670
Sonnentrucker, P., Cami, J. Ehrenfreund, P., & Foing, B. H. 1997, A&A, 327, 1215
Tuairisg, S.Ó., Cami, J., Foing, B. H., Sonnentrucker, P., & Ehrenfreund, P. 2000, A&AS, 142, 225
van Dishoeck, E. F., & Black, J. H. 1986, ApJS, 62, 109
Vuong, M. H., & Foing, B. H. 2000, A&A, 363, L5
Walker, G. A. H., Webster, A. S., Bohlender, D. A., & Krełowski, J. 2001, ApJ, 561, 272
Wang, S., et al. 2003, Proc. SPIE, in press
Welty, D. E., & Hobbs, L. M. 2001, ApJS, 133, 345
Weselak, T., Schmidt, M., & Krełowski, J. 2000, A&AS, 142, 239